Early mouse ovarian follicles develop into a thecal cell network that generates androgens during peri-puberty

Authors: Qi Yin[1], Allan C Spradling[1]*

Affiliations:

[1]Howard Hughes Medical Institute Research laboratories, Department of Biosphere Sciences, Carnegie Institution for Science, Baltimore, MD 21218, USA

*Corresponding author. Email: spradling@carnegiescience.edu

Abstract: The earliest mouse fetal ovarian follicles (wave 1) grow rapidly in the ovarian medulla but their function remains unclear. We found these follicles do not produce mature oocytes but follow a distinct developmental program. At preantral stages, their oocytes and then most granulosa cells turn over. Thecal cells expand further, vascularize, express androgen biosynthetic genes, consistent with scRNAseq analyses. In contrast, normal follicles begin to arise during week two from primordial follicles near the medullar-cortical boundary with mosaic granulosa cells. The highest levels of androgen biosynthetic gene expression occur in the thecal network at 5 weeks, a period known as "peri-puberty," and may influence sexually dimorphic brain development and reproductive behavior. Abnormalities of thecal network formation or function in humans may contribute to polycystic ovarian syndrome.

INTRODUCTION

In mice, humans and other mammals which lack female germline stem cells, the production of ovarian follicles (an oocyte surrounded by somatic granulosa cells) takes place in well-defined sequential steps within the fetal and early juvenile ovary (reviews: Edson et al. 2009; Rotgers et al. 2018; McKey et al. 2022). During mouse fetal development, migrating primordial germ cells (PGCs) arrive at the ovary beginning at embryonic day 10.5 (E10.5) and interact with bipotential pregranulosa cells (BPGs) derived from precursors in the gonadal primordium (Hirshfield, 1992; Mork et al., 2012; Figure 1A). Subsequent events generate two recognized subclasses of ovarian follicles. As PGCs develop into germline cysts and enter meiosis, BPGs surround them to found "wave 1" ovarian follicles that persist in the ovarian medulla. However, distinct progenitors in the coelomic epithelium soon generate epithelial pregranulosa cells (EPGs) that over time displace BPGs from most follicles outside the medulla, giving rise to "wave 2" follicles which populate the ovarian cortex (Mork et al., 2012; Zheng et al., 2014a; Niu and Spradling, 2020). Wave two follicles become quiescent primordial follicles shortly after birth. During postnatal (P) life, small groups of these follicles periodically activate and grow in response to nutritional and gonadotrophin signals to sustain lifelong fertility.

Once activated, follicular granulosa cells (GCs) start to proliferate within the monolayer covering primary follicles and soon form multiple GC layers surrounding the oocyte (Habara et al., 2021; Figure S1A-D). The oocyte in such secondary follicles sends GDF9 signals that induce its granulosa cells to attract ovarian mesodermal precursors that differentiate into thecal cells and synthesize steroid hormones (review Richards et al. 2017). Additionally, ovarian medullary precursors generate thecal fibroblastic cells and perivascular smooth muscle cells that vascularize the thecal region and enable such follicles to collectively serve as a major systemic steroid hormone source (Guzmán et al. 2023). An ovarian type type closely related to thecal cells, interstitial gland cells, also coordinately forms in mice and many other mammals (Jiménez,

2009; Miyabayashi et al. 2015). Nr5a2/Lrh1 is differentially expressed in BPGs compared to EPGs in wave 1 follicles and promotes thecal cell vascularization that is essential for ovulation (Duggavathi et al. 2008; Bianco et al. 2019; Guzmán et al. 2022). Two classes of steroid hormone-producing Leydig cells, fetal and adult, also arise in the developing testis but how they relate to thecal cell production remains unclear (Miyabayashi et al. 2015; Liu et al. 2016).

Follicular cells synthesize specific steroid hormones during their development. Thecal steroidogenic cells of late secondary and preantral follicles convert cholesterol to androgens through a series of enzymatic reactions involving steroidogenic acute regulatory protein (StAR), cytochrome P450 family 11 subfamily A member 1 (CYP11A1), hydroxy-delta-5-steroid dehydrogenase, 3 beta- and steroid delta-isomerase 1 (HSD3B1), cytochrome P450 family 17 subfamily A member 1 (CYP17A1), and steroid 5 alpha-reductase 1 (SRD5A1) (Richards et al. 2017). Ovarian androgen production by thecal cells during juvenile development is essential for normal maturation and puberty onset (Walters et al., 2019; Kelava et al., 2022). In addition, thecal androgens diffuse into neighboring GCs, where they are converted into estrogen by the action of hydroxysteroid 17-beta dehydrogenase 1 (HSD17B1) and cytochrome P450 family 19 subfamily A member 1 (CYP19A1). Estrogen produced in this manner signals the hypothalamus to initiate gonadotrophin production and is essential for subsequent follicular maturation. After ovulation, the oocyte-free follicle is modified into a corpus luteum, and its thecal cells undergo luteinization to generate progesterone (Edson et al. 2009).

Separate groups ("waves") of immediately developing and arrested follicles are produced in many mammalian and vertebrate species (Browning, 1973; Hirshfield, 1992; Gougeon, 1996; DeFalco and Capel, 2009). However, the function of murine wave 1 follicles has remained a matter of debate. Wave 1 follicles secrete anti-Müllerian hormone (Amh) that likely delays and helps control wave 2 follicular activation (Meinsohn et al. 2021). Some wave 1 follicles undergo process of atresia, and some were proposed to synthesize steroid hormones (Ojeda et al. 1986;

Galas et al. 2012; Findlay et al. 2015; Zheng et al. 2014b). Based on lineage tracing of Foxl2-expressing pre-granulosa cells, wave 1 follicles were suggested to generate a substantial number of fertile oocytes during the first two months of fertility (Zheng et al. 2014a). Here we show that most wave 1 follicles lose their oocytes and granulosa cells after which their thecal cells develop into a stromal network highly enriched in androgen biosynthetic gene expression during peri-puberty. Moreover, we found that a small third follicle subclass, "wave 1.5," acquire a mosaic covering of both BPG and EPG-like GCs near the cortex/medullar border. Wave 1.5 follicles begin to activate by postnatal week 2, and probably produce most fertile oocytes at puberty, rather than wave 1 or the first re-activated wave 2 follicles.

RESULTS

Wave 1 follicle development

Advances that allow tissue clearing (Faire et al., 2015; Feng et al., 2017; Fiorentino et al., 2020; McKey et al., 2022), make it possible to image the entire mouse ovary without sectioning. To better understand wave 1 follicle development, we employed a clearing-enhanced 3D (Ce3D) method to analyze wild type C57BL/6J ovaries at the cellular level after whole-mount staining (Li et al., 2017) as well as analyzing sectioned material (Figure S1). Multiple ovaries were reconstructed during weeks (wks) 1-5 of development (Table 1) and as indicated. In C57BL/6J mice, puberty (peri-puberty) typically occurs between 4 and 5 wks of age, but the first ovulation, which signals sexual maturity, doesn't take place until 7 wks (Figure 1B) (Nelson et al., 1990; Zhou et al., 2007).

Using these tools we characterized the development of wave 1 follicles. Wave 1 follicles begin to grow as primary follicles near the time of birth based on gene expression (Niu and Spradling, 2020). By P10 we counted about 3,300 total follicles (Figure 1C; Figure S1E-G) and 278-293 wave 1 follicles (Figure 1D; Figure S1E-G); wave 1 oocyte volume increased during wk 1-wk3 (Figure 1E). By 2 wks, many wave 1 follicles in the medulla contained 2-4 layers of GCs and 1-2 thecal cell layers, appearing as normal secondary follicles (Figure S1A-D, G) .

Wave 1 follicles undergo remodeling

Beginning by 3 wks, wave 1 follicles began to leave the normal developmental pathway and remodel, changes that have traditionally been attributed to whole follicle degeneration known as "atresia" (Figure S2). These follicles were first identified due to oocyte loss, initially leaving behind nearly intact granulosa and thecal cell layers (Figure 1F; Figure S2A,B). The non-canonical follicles become reduced in size and retain a hole beneath the granulosa cell layer where the oocyte had been located. Oocyte loss from wave 1 follicles increases further by 4 weeks, and exceeds 80% by 5 wks (Figure S2A,B; Figure 1F). Examination in the electron

microscope revealed that the holes retain the oocyte's zona (ZP) for a considerable period, which may stabilize them (Figure S2C). Thus, the great majority of wave 1 follicles lose their oocytes prior to puberty and do not contribute to early ovulation.

The loss of oocytes from most wave 1 follicles was not due to classical atresia, as expected if these follicles contained developmental or meiotic defects. Instead, the remodeling appears to be a developmental process in which most or all thecal cells are retained while oocytes and most granulosa cells are lost. Documenting the nature of wave 1 follicle remodeling was assisted by tracing cell lineages. We used Foxl2-CreERT2 mice to selectively lineage label GCs associated with wave 1 follicles (Figure 2A; Mork et al. 2012; Zheng et al. 2014a) and to follow their behavior during follicle remodeling (Figure 2). Following brief administration of Tamoxifen at embryonic day 16.5 (E16.5), most wave 1 follicles showed mosaic EYFP-labeling of GCs at 2 wks while cortical wave two follicle granulosa cells were unlabeled (Figure 2B, C). By 5 wks the number of follicles with Ddx4-positive oocytes and normal granulosa layers had decreased to a mean of 26 (Figure 2D, E). Remodeled follicles lost 94% of their granulosa cells compared to 3 wk wave 1 follicles prior to remodeling, retaining an average of only 14 such cells, located adjacent to the hole (Figure 2F). As part of remodeling, wave 1 oocyte holes decreased in size and clustered in medulla (Figure 2F, arrowheads; Figure S2A,B).

These experiments also identified a new subclass of primordial follicles located near the medulla-cortex boundary (Figure S3). Whether assayed with tdTomato (Figure S3A-D) or EYFP (Figure S3E-G), Foxl2-CreERT2 activation by Tx injection at E16.5 labels not only wave 1 medullar follicle GCs, but at 2 wks it labels a small subset of primordial follicles near the cortex-medulla boundary that contain 1 or a few positive granulosa cells (Figures S3C-E). Overall, a mean of 421 such "wave 1.5" follicles were identified among 5,843 total follicles (Figure S3F). (A small number of primordial follicles containing one or a few EYFP-positive GCs appeared in this same location even when Tx was injected at E12.5 or E14.5, rather than E16.5). Wave 1.5

follicles begin to develop shortly after 2 wks since nearly 70% of normal secondary follicles in 5 wk ovaries contained EYFP-positive GCs (Figure S3H). More than 70% of pre-antral or later follicles contained EYFP GCs up to at least 5 wks (Figure S3I).

Developing wave 1 follicles retain thecal cells and expand their number

Further lineage marking revealed that steroidogenic thecal cells (STCs) remain associated with remodeling wave 1 follicles and increase in number (Figure 3). We validated that thecal cells strongly express the steroid biosynthetic enzyme Cyp17a1 at 3 wks using immunofluorescent staining (Figure S4A). Consequently, we used the Cyp17a1 gene to drive optimized Cre (iCre) and activate CAG-tdTomato (Figure 3A) to mark STCs. In 2 wk ovaries, tdTomato expression was observed in thecal cells sheathing large medullar follicles (Figure 3B,C). Additional cells that appear to be interstitial gland cells also become labeled between many follicles (Figure S4B,C; arrows). During wave 1 follicle development from 2 wks to 5 wks, the number of tdTomato-labeled cells associated with nuclear holes dramatically increases (compare Figure 3D to 3E). Some granulosa cells (GCs) may also become labeled initially (Figure S4C, arrowheads) perhaps because GC precursor cells briefly express Cyp17a1 during embryonic stages. Because, most GCs turn over as part of wave 1 remodeling (Figure 2D) the multiple, nearly uniform groups of tdTomato-positive cells associated with remodeled wave 1 follicles by 5 wk represent abundant STCs and interstitial gland cells containing subcellular features associated with steroid production. Oil red staining documented abundant lipid droplet accumulation in these cells from 2 wks to 5 wks (Figure 3F,G). These cells express the steroidigenic proteins HSD3B1, and PLIN1 (Figure 3H). Electron microscopy confirmed that expanded wave 1 follicular cells display distinctive lipid droplets and mitochondria characteristic of thecal and interstitial gland cells (Figure 3I; Figure S4E).Wave 1 follicle remodeling by 5 wks has generated a cellular network (Figure 3J), which persists within the ovary after 5 wks (Figure S4D).

Mapping cell transcription during juvenile ovary development

To gain more insight into wave 1 follicle development and remodeling, we analyzed gene expression in single cells from ovaries every wk from wk2 to wk6 (Figure 4A). 31 initial clusters (c0-c30) were identified, comprising nine major cell group (Figure 4A'), based on their expression of well known marker genes (Figure S5). These comprised granulosa cells (Amhr2, Poole et al., 2016), stromal cells (Mfap4, Morris et al., 2022), thecal cells (Cyp17a1, Young and McNeilly, 2010), hematopoietic cells (Runx3, Boto et al., 2018), endothelial cells (Cldn5, Richards et al., 2022), pericytes (Notch3, Wang et al., 2014), smooth muscle cells (Acta2, Rockey et al., 2013), and epithelial cells (Upk3b, Niu and Spradling, 2020). In addition, three clusters exhibited low UMIs, and were excluded them from subsequent analysis, as was cluster15 due to the presence of suspected doublets. Because germ cells make up only a small fraction of the total cell population, a germ cluster was not detected.

We re-clustered the ten initial granulosa cell clusters in Seurat, yielding 18 new clusters gc0-gc17; (Figure 4B) and classified them into groups corresponding to their likely association with primordial (gc11), primary (gc3, gc8), secondary (gc1, gc4, gc9), antral (gc2, gc7, gc10, gc13), and reorganizing (gc0, gc6) follicles, as well as mitotically cycling cells (Figure 4B'; Figure S5C). Surprisingly, even wk 2 ovaries contained cells from all clusters except for antral clusters gc6, and gc13. These likely represent GCs on the most mature follicles. We identified up to 250 top differentially expressed genes for each group (see Supplemental Dataset 5) to enable Metascape Analysis (Zhou et al. 2019).

Analysis of GCs covering primordial follicles in cluster gc11, identified multiple genes that may be involved in quiescence. For example, Mndal has been implicated in suppressing cell growth (Zhang et al., 2009), while the high expression of Aldh1a2 supports a possible role for retinoic acid in the GCs of primordial follicles. Metascape analysis of the top 250 genes selectively expressed in gc11 identified significant matches to multiple negative regulatory

pathways that may suppress vasculature development (Supplementary Dataset 5). The relative absence of blood vessels in the ovarian cortex compared to the medulla is well known, and a low nutritional microenvironment is thought to promote follicular quiescence (see Edson et al. 2009). Our results suggest that such suppression may be actively influenced by primordial granulosa cells. The number of GCs recovered on primordial follicles decreased sharply from 2-6 wks (Figure 4E), but this likely reflects the proliferation of GCs on developing follicles, rather than an absolute decrease in the ovarian reserve.

The putative remodeling follicle clusters gc0 and gc6 had the potential to reveal regulatory mechanisms controlling wave 1 follicle development. Consistent with a connection to wave 1, the number of gc0 and gc6 cells is low at 2 and 3 wks but jumps 9.8-fold at wk 4 (Supplemental Dataset 6). Preferentially expressed genes in gc0 and gc6 include Cyp1b1, Atf3, Cxcl1, Bmp2, Apoe and Sox4. Metascape analysis identified vasculature development (-7.7; -4.0) cell cycle (-6.7; -9.2) , and positive regulation of programmed cell death (-4.1; -4.9), where the numbers indicate (q values log10 for gc0; gc6). These findings suggest genes and pathways by which GCs on remodeling wave 1 follicles attract thecal cells, stimulate vasculature development, and stimulate GC population turnover.

Analysis of selected mesenchymal cells

The first two thecal layers located just outside the GC basement membrane ("theca interna") are enriched in STCs. The outer "theca externa" is enriched in angiogenic cells, blood vessels, and fibroblastic cells. The diverse remaining scRNA cell groups in the initial clustering include thecal, stromal, smooth muscle, endothelial, blood cells and other cells likely to be present on normal and remodeled thecal layers (Figure 4A'). Consistent with this, endothelial cells expressing Flt1 (c22) and blood cells expressing Laptm5 (c23), increased nearly 4-fold between wk3 and wk5, consistent with network vascularization. We re-clustered the

mesenchymal and stromal cells (Figure 4A) yielding 21 new clusters to pursue a higher resolution picture of thecal expansion (Figure 4A'; Figure S5D). The re-clustered mesenchymal cells fell into eight groups, STCs expressing Cyp17a1, Tagln-expressing fibroblasts (Sun et al., 2023), Col14a1-expressing fibroblasts (Xie et al., 2018), Cd24a-expressing fibroblasts (Wang et al., 2022), Cxcl14-expressing fibroblasts (Sjoberg et al., 2019), Hox9-expressing fibroblasts (Khoa et al., 2001, and mitotic cells expressing Mki67 (Figure 4C, C').

Two clusters were identified as thecal cells, g9 and g11, due to expression of Nr5a1 (Miyabayashi et al. 2015) and androgen biosythentic genes (Figure 4D). The number of g9 cells increased 4.1-fold between wk3 and wk5 (Supplemental Dataset 6), expressed steroidigenic gene transcripts whose levels peaked at wk 5, and probably correspond to follicle-associated thecal cells. In contrast, g11 cell number was higher than g9 at 2 wks, but remained nearly constant, suggesting they correspond to interstitial gland cells which are forming by 2 wk (Figure 3B) before the large thecal cell expansion. Thecal cells initially lack LH receptor encoded by the Lhcgh gene and can form in FSH deficient mice (Kumar et al. 1997). The levels of androgenic gene expression we observed in both clusters g9 and g11 correlated with their Lhcgh expression levels, suggesting that steroidigenic gene expression remains under gonadotrophin control (Figure S6A).

Increased vascularization such as occurs during thecal expansion is often regulated by signaling molecules such as vascular endothelial growth factors (Vegfa-d) and angiopoietins (Angpt1 and Angpt2). The expression of Flt1, the receptor for VEGFs and Tek, the receptor for Angpt1 and Angpt2, was fairly constant and highly enriched in endothelial cells throughout wk2-wk6 of ovary development. The ratio of Angpt1 and its antagonist Angpt2 changed relatively little. However, Vegfa and Vegfb expression is widespread, and peaks at wk5 in thecal cells (g9). The actin-crosslinking gene transgelin (Tgln) marks smooth muscle and is involved in vascular smooth muscle expansion during angiogenesis, often downstream from Vegf (Tsjui-

Tamura et al. 2021). Four mesenchymal clusters expressed Tagln highly, making their roles hard to distinguish, but expression of Tagln in g17 reached the highest levels and peaked during wk4 and wk5. Cluster g16 was adjacent to the g9 and g11 thecal cell clusters in the UMAP plot and its enriched genes elicited GO terms related to blood vessel development as well as steroid hormone biosynthesis (Supplemental Dataset 4), suggesting these cells contribute in some way to thecal network formation.

Wave 1 follicles may enhance androgen production during puberty

Steroidogenesis primarily takes place in STCs and GCs (Figure 4D). Among the key genes involved, including Star, Cyp11a1, Cyp17a1, Cyp19a1, and Hsd17a1, the first three are expressed in the STCs, while the latter two are expressed in the GCs. Hsd3b1 is expressed in both GCs and STCs. STCs expressing Cyp11a1, Hsd3b1, and Cyp17a1, increased in number from 2 wks to 5 wks, consistent with the Cyp17a1 lineage tracing and staining results. Star, a crucial gene responsible for transporting cholesterol from the cytoplasm into mitochondria, is essential for steroidogenesis. The percentage of STCs expressing Star increased from approximately 50% to over 80% at wk 5 (Figure 4D). Our findings demonstrate that STCs increase in number, and acquire a full complement of androgen biosynthetic enzymes during peri-puberty. In contrast, a full complement of cells capable of significant estrogen production may not arise until wk 6 (Figure 5D), consistent with estrogen levels lagging androgen levels during puberty (Galas et al. 2012; Trova et al. 2021).

DISCUSSION

The developmental fate of early follicles

The earliest wave of ovarian follicles in many mammals including humans reaches advanced stages much sooner than would be necessary to support the first ovulation. In rodents this wave 1 follicular group was thought to undergo atresia rather than ovulate (Hirshfield and

DeSanti, 1995; Gougeon 1996; McGee and Hsueh, 2000; Eppig and Handel, 2012). However, lineage marking of Foxl2-expressing granulocytes with GFP at E16.5 showed that follicles with labeled granulosa cells, presumed to be entirely of wave 1 origin, constituted all antral or older follicles up to sexual maturity. Many of these follicles ovulated during the first two months of fertility suggesting that wave 1 follicles contribute substantially to offspring even as they are gradually replaced by wave 2-derived follicles (Zheng et al. 2014a; review Zheng et al. 2014b).

The results presented here are consistent with the experimental data of Zheng et al. 2014a) but lead to a modified conclusion (Figure 5A). In addition to 225-250 wave 1 follicles in the medulla that activate at birth, we identified at least 400 wave primordial follicles near the medullar-cortical border that are labeled with Foxl2-Cre at E16.5 and appear to begin development by P14. Although germ cells are surrounded by somatic cells in EMs beginning at E10.5, we know relatively little about the early interactions of BPGs with development germline cysts. Wave 1.5 primordial follicles may arise because the apparent replacement of BPGs with EPGs during fetal development (Niu and Spradling, 2020) is not complete near the boundary, generating follicles with a mosaic covering of both cell types. This is consistent with a report that individual granulosa cells in border region follicles variably express the BPG-marker gene Nr5a2 (Meinsohn et al. 2021). Alternatively, a few EPGs on primordial follicles in this junction region may activate Foxl2 early due to the border microenvironment. Regardless of the mechanism, these follicles as well as true wave 1 follicles were labeled in our Foxl2 lineage tracing experiments, and presumably those of Zheng et al. 2014a). "Wave 1.5" follicles start to grow as early as 2 wks and produce most of the first follicles to develop fully, ovulate and generate offspring (Figure S3).It remains possible that a small number of wave 1 follicles, ~25 or fewer, resist remodeling, and/or that a small number of early activated wave 2 follicles, which we did not detect, are ovulated shortly after sexual maturity. However, their contribution to fertility, if any, appears to be minor. Thus, wave 1.5 rather than wave 1 follicles are responsible for most

early fertility, while wave 2 follicles serve almost entirely as the ovarian reserve and only begin to activate between puberty and sexual maturity, possibly in concert with the onset of pulsatile HPE axis activity (Figure 5A).

Wave 1 follicles generate a thecal cell network that synthesizes androgens during peri-puberty.

Our experiments suggest a different reason for why many mammals generate two waves of follicles containing distinctive granulosa cells. Wave 1 follicles undergo a developmental remodeling process reminiscent of corpus luteum formation that converts these follicles into an androgen-producing network (Figure 5B). At least 90% of the approximately 250 wave 1 follicles follow this pathway. After oocyte loss and granulosa cell reduction, thecal cell proliferation may be stimulated, due to reduced GC inhibitory signals. They generate a distinctive region in the central medulla, "the thecal network" recognizable by the residual wave 1 oocyte holes, and enrichment of thecal and interstitial gland cells (Figures 2F; 3D; S2B,C; S4; Supplemental movies). Production of a thecal network may occur in response to the low early juvenile gonadotrophin and hormonal milieu encountered by wave 1 follicles as they grow beginning at P1. However, conditions conducive to wave 1 remodeling probably may not last long, since wave 1.5 primordial follicles activated beginning just 2 wks later are mostly able to develop normally and produce offspring. Modifying wave 1 follicular development into a network of thecal and interstitial gland cells likely increases androgen production during peri-puberty and may be a previously unrecognized additional variation of follicular steroidogenesis, like follicle remodeling after ovulation into the corpus luteum to generate progesterone.

While previous studies have occasionally acknowledged the shared origin of STCs and interstitial glands, there has been a persistent view that these are distinct cell groups that happen to express similar patterns of genes involved in steroidogenesis such as Cyp17a1 (Miyabayashi et al., 2015). Our studies suggest that interstitial gland cells begin to arise in association with

wave 1 follicles (Figure 3B, Figure 3C, arrow), persist as thecal cells increase during remodeling (Figure 3D) and remain between former follicles in the thecal network (Figure 3J).

Steroid hormones mediate sexual development in juvenile mice and during peri-puberty

Steroid hormones influence the development of sexually dimorphic organs including the brain (review Simerey, 2002; Arnold, 2009). They have multiple sources, including steroids in the maternal circulation during pregnancy, as well as subsequent systemic and local steroid production during juvenile stages. Wave 1-derived thecal cell numbers are high during wk 4-5 of juvenile development. a period known as peri-puberty that has been associated with sexual behavior development and with high levels of androgens, as well as relatively low estrogen production (Trova et al. 2021). While the sensitivity of the brain to steroid influences is probably declining during this period, sexually dimorphic circuits are still being shaped in a manner that is important for sexually dimorphic behaviors in female and male rodents (Sisk and Zehr, 2005; Templin et al. 2019; Trova et al. 2021). Potential targets of this influence include the anteroventral periventricular nucleus (AVPV) which is larger in female than male rodents, and helps regulate female reproductive functions such as ovulation and gonadotrophin production. Sex hormones produced in females during puberty also enhance cell death in the primary visual cortex, reducing its volume in females compared to males.

Functions of the wave 1 thecal network

Conditions that alter the number of wave 1 follicles might provide clues to their function. In Turner syndrome, wave 1 follicle development is significantly reduced (Miura et al. 2017). This imbalance might might decrease androgen levels, potentially affecting juvenile development. Consistent with hormonal disruption, hormone replacement therapy significantly improves the development of individuals with Turner syndrome (Klein et al., 2018). Moreover,

androgens are known to play an important role in this effect (Zuckerman-Levin et al., 2009; Viuff et al., 2022).

We examined mouse X/O individuals and looked for changes in wave 1 follicle numbers (Figure S6B-C). In our experiments, wave 1 follicle numbers were reduced relative to levels in X/X control females at wk1 of development. However, the reduction was transient and by 2 wks, still before remodeling and thecal cell expansion, X/O and X/X females had similar wave 1 follicles numbers. Consequently, we could not draw any conclusions regarding the functional role of wave 1 follicles and their remodeling.

The normal fate of the wave 1 thecal network is of considerable interest, since relatively high androgen levels do not persist during adulthood (Trova et al. 2021). The scRNAseq data suggested that androgen biosynthetic enzyme mRNAs per thecal cell decreased by 6 wks. However, thecal network cells likely remain since Cyp17a1 lineage staining persisted in the medulla at least until wk 7 (Figure S4C). Wave 2-derived follicles constitute 10% of growing follicles (but 0% of antral follicles) at puberty and 20% of growing follicles at sexual maturity (Zheng et al. (2014a). A decrease in androgenic enzymes without reduced cell numbers suggests that androgen production may normally be downregulated after puberty.

Do human wave 1 follicles follow an analogous developmental pathway?

Our studies are likely to be relevant to the behavior of early human ovarian follicles, which as in mice begin developing long before any need for ovulation. Puberty in human females typically commences between the ages of 8 to 13 years, whereas antral follicles are present even in human fetuses and infants just a few months old and continue to be produced during juvenile life. Early follicles in humans, like in mice, might undergo remodeling to enhance production of androgens or other steroid hormones that sex-specifically influence organ and brain development (Cui et al., 2013; Bell, 2018).

Wave 1 follicle remodeling and polycystic ovarian syndrome

Our findings may be relevant to the origin and high frequency of polycystic ovary syndrome (PCOS) (MacCartney and Marshall, 2016). Our results revealed that the mouse ovary normally generates a PCOS-like state within a limited and biologically defined follicular subgroup- wave 1 follicles, that end up forming a stromal network within the ovarian medulla. Wave 1 follicles remodel into cyst-like structures (i.e. lacking oocytes) with reduced granulosa layers but expanded thecal cells producing androgens. Similar follicular characteristics have consistently been observed in the ovaries of individuals with PCOS (Chang, 2007; Franks and Hardy, 2010; review- Walters et al. 2012).

Several situations might alter the number of follicles undergoing a wave 1-like fate. Low levels of steroid hormones and gonadotrophins, or unknown signals, during the first few wks of juvenile life when wave 1 follicles normally begin developing may provide a transient window that triggers this alternative pathway. Follicles that activate development even two wks later return to the normal pathway, and act to establish normal cyclicity after a brief period of relatively high androgen production during puberty. PCOS might result from several types of changes to this scenario, leading to its high frequency. Inductive conditions might persist too long sending later activated follicles in addition to wave 1 follicles along the remodeling pathway. Processes needed to downregulate androgen biosynthetic gene expression in a timely manner within existing network thecal cells might also be susceptible to delay, including by epigenetic or environmental factors. Critically, our results indicate that further studies of wave 1 follicle induction and regulation in mice, and in other mammalian systems, have significant potential to advance our understanding of this common problem, and to identify interventions able to ameliorate it.

REFERENCES

Bell MR (2018). Comparing Postnatal Development of Gonadal Hormones and Associated Social Behaviors in Rats, Mice, and Humans. Endocrinology 159, 2596-2613. doi: 10.1210/en.2018-00220.

Bianco S, Bellefleur AM, Beaulieu É, Beauparlant CJ, Bertolin K, Droit A, Schoonjans K, Murphy BD & Gévry N (2019). The ovulatory signal precipitates LRH-1 transcriptional switching mediated by differential chromatin accessibility. *Cell Reports* **27** 2443.e4–2454.e4. (https://doi. org/10.1016/j.celrep.2019.07.088)

Boto P, Csuth TI, Szatmari (2018). I. RUNX3-Mediated Immune Cell Development and Maturation. Crit Rev Immunol. 38, 63-78. doi: 10.1615/CritRevImmunol.2018025488.

Browning HC (1973). The evolutionary history of the corpus luteum. Biology of Reproduction 8, 128-137.

Cui J, Shen Y, Li R. (2013). Estrogen synthesis and signaling pathways during aging: from periphery to brain. Trends Mol Med. 19, 197-209. doi: 10.1016/j.molmed.2012.12.007.

DeFalco T, Capel B (2009). Gonad morphogenesis in vertebrates: divergent means to a convergent end. Annu. Rev. Cell Dev. Biol. 25, 457-482.

Duggavathi R, Volle DH, Mataki C, Antal MC, Messaddeq N, Auwerx J, Murphy BD & Schoonjans K **(**2008). Liver receptor homolog 1 is essential for ovulation. *Genes and Development* **22** 1871–1876. (https://doi. org/10.1101/gad.472008)

Edson MA, Nagaraja AK, Matzuk MM. (2009). The mammalian ovary from genesis to revelation. Endocr Rev. 30, 624-712. doi: 10.1210/er.2009-0012.

Eppig JJ, Handel MA. (2012). Origins of granulosa cells clarified and complexified by waves. Biol Reprod 86, 34. doi: 10.1095/biolreprod.111.096651.

Faire M, Skillern A, Arora R, Nguyen DH, Wang J, Chamberlain C, German MS, Fung JC, Laird DJ. (2015). Follicle dynamics and global organization in the intact mouse ovary. Dev Biol. 403, 69-79. doi: 10.1016/j.ydbio.2015.04.006.

Feng Y, Cui P, Lu X, Hsueh B, Möller Billig F, Zarnescu Yanez L, Tomer R, Boerboom D, Carmeliet P, Deisseroth K, Hsueh AJ. (2017). CLARITY reveals dynamics of ovarian follicular architecture and vasculature in three-dimensions. Sci Rep. 7, 44810. doi: 10.1038/srep44810.

Findlay JK, Hutt KJ, Hickey M, Anderson RA. (2015). How Is the Number of Primordial Follicles in the Ovarian Reserve Established? Biol Reprod. 93, 111. doi: 10.1095/biolreprod.115.133652.

Fiorentino G, Parrilli A, Garagna S, Zuccotti M. (2020). Three-Dimensional Micro-Computed Tomography of the Adult Mouse Ovary. Front Cell Dev Biol. 8, 566152. doi: 10.3389/fcell.2020.566152.

Galas J, Slomczynska M, Knapczyk-Stwora K, Durlej M, Starowicz A, Tabarowski Z, Rutka K, Szoltys M. (2012). Steroid levels and the spatiotemporal expression of steroidogenic enzymes and androgen receptor in developing ovaries of immature rats. Acta Histochem 114, 207–216.

Gougeon A. (1996). Regulation of ovarian follicular development in primates: facts and hypotheses. Endocr Rev 17:121–155. doi: 10.1210/edrv-17-2-121. PMID: 8706629

Guzmán A, Hughes CHK, Murphy BD (2022). Liver receptor homolog 1 (LHR-1) regulates follicle vasculature during ovulation in mice. Reproduction 164, 283-289.

Guzmán A, Hernández-Coronado CG, Gutiérrez CG, Rosales-Torres AM. (2023). The vascular endothelial growth factor (VEGF) system as a key regulator of ovarian follicle angiogenesis and growth. Mol Reprod Dev. 90, 201-217. doi: 10.1002/mrd.23683.

Habara O, Logan CY, Kanai-Azuma M, Nusse R, Takase HM (2021). WNT signaling in pre-granulosa cells is required for ovarian folliculogenesis and female fertility. Development. 148, dev198846. doi: 10.1242/dev.198846.

Hatzirodos N, Hummitzsch K, Irving-Rodgers HF, Rodgers RJ. (2015). Transcriptome comparisons identify new cell markers for theca interna and granulosa cells from small and large antral ovarian follicles. PLoS One. 10, e0119800. doi: 10.1371/journal.pone.0119800.

Hirshfield AN. (1992). Heterogeneity of cell populations that contribute to the formation of primordial follicles in rats. Biol Reprod 47:466–472.

Hirshfield AN, DeSanti AM. (1995). Patterns of ovarian cell proliferation in rats during the embryonic period and the first three weeks postpartum. Biol Reprod 1995;53:1208 –1221.

Jiménez R (2009). Ovarian organogenesis in mammals: mice cannot tell us everything. Sex Dev. 3, 2911-301.

Kelava I, Chiaradia I, Pellegrini L, Kalinka AT, Lancaster MA. (2022). Androgens increase excitatory neurogenic potential in human brain organoids. Nature 602, 112-116. doi: 10.1038/s41586-021-04330-4.

Khoa ND, Nakazawa M, Hasunuma T, Nakajima T, Nakamura H, Kobata T, Nishioka K. (2001). Potential role of HOXD9 in synoviocyte proliferation. Arthritis Rheum. 44, 1013-21. doi: 10.1002/1529-0131(200105)44:5<1013::AID-ANR180>3.0.CO;2-O.

Klein KO, Rosenfield RL, Santen RJ, Gawlik AM, Backeljauw PF, Gravholt CH, Sas TCJ, Mauras N (2018). Estrogen Replacement in Turner Syndrome: Literature Review and Practical Considerations. J Clin Endocrinol Metab. 103, 1790-1803. doi: 10.1210/jc.2017-02183.

Kumar TR, Wang Y, Lu N, Matzuk MM. (1997). Follicle stimulating hormone is required for ovarian follicle maturation but not male fertility. Nat Genet. 15, 201-4. doi: 10.1038/ng0297-201.

Li W, Germain RN, Gerner MY. (2017). Multiplex, quantitative cellular analysis in large tissue volumes with clearing-enhanced 3D microscopy (Ce3D). Proc Natl Acad Sci U S A. 114, E7321-E7330. doi: 10.1073/pnas.1708981114.

Liu C, Rodriguez K, Yao HHC. Mapping lineage progression of somatic progenitor cells in the mouse fetal testis. Development. 2016;143(20): 3700–3710.

McGee EA, Hsueh AJ. (2000). Initial and cyclic recruitment of ovarian follicles. Endocr Rev 21:200–214. doi: 10.1210/edrv.21.2.0394.

McKey J, Anbarci DN, Bunce C, Ontiveros AE, Behringer RR, Capel B. (2022). Integration of mouse ovary morphogenesis with developmental dynamics of the oviduct, ovarian ligaments, and rete ovarii. Elife 11, e81088. doi: 10.7554/eLife.81088.

Meinsohn MC, Saatcioglu HD, Wei L, Li Y, Horn H, Chauvin M, Kano M, Nguyen NMP, Nagykery N, Kashiwagi A, Samore WR, Wang D, Oliva E, Gao G, Morris ME, Donahoe PK, Pepin D. (2021). Single-Cell sequencing reveals suppressive transcriptional programs regulated by MIS/AMH in neonatal ovaries. PNAS 118, 20. doi: https://doi.org/10.1073/pnas.2100920118,

Miura K, Murata C, Harikae K, Suzuki H, Kanai-Azuma M, Kurohmaru M, Tsunekawa N, Kanai Y. (2017). Defects in the first wave of folliculogenesis in mouse XO ovaries. J Reprod Dev. 63, 333-338. doi: 10.1262/jrd.2017-033.

Miyabayashi K, Tokunaga K, Otake H, Baba T, Shima Y, Morohashi K. (2015). Heterogeneity of ovarian theca and interstitial gland cells in mice. PLoS One. 10, e0128352. doi: 10.1371/journal.pone.0128352.

Mork L, Maatouk DM, McMahon JA, Guo JJ, Zhang P, McMahon AP, Capel B (2012). Temporal differences in granulosa cell specification in the ovary reflect distinct follicle fates in mice. Biol Reprod. 86, 37. doi: 10.1095/biolreprod.111.095208.

Morris ME, Meinsohn MC, Chauvin M, Saatcioglu HD, Kashiwagi A, Sicher NA, Nguyen N, Yuan S, Stavely R, Hyun M, Donahoe PK, Sabatini BL, Pépin D. (2022). A single-cell atlas of the cycling murine ovary. Elife 11, e77239. doi: 10.7554/eLife.77239.

Nelson JF, Karelus K, Felicio LS, Johnson TE (1990). Genetic influences on the timing of puberty in mice. Biol Reprod. 42, 649-55. doi: 10.1095/biolreprod42.4.649.

Niu W, Spradling AC (2020). Two distinct pathways of pregranulosa cell differentiation support follicle formation in the mouse ovary. Proc Natl Acad Sci U S A. 117, 20015-20026. doi: 10.1073/pnas.2005570117.

Ojeda SR, Urbanski HF, Ahmed CE. (1986). The onset of female puberty: studies in the rat. Rec Prog Horm Res 42:385–442.

Poole DH, Ocón-Grove OM, Johnson AL. (2016). Anti-Müllerian hormone (AMH) receptor type II expression and AMH activity in bovine granulosa cells. Theriogenology 86, 1353-60. doi: 10.1016/j.theriogenology.2016.04.078.

Richards JS, Ren YA, Candelaria N, Adams JE, Rajkovic A. (2017). Ovarian Follicular Theca Cell Recruitment, Differentiation, and Impact on Fertility. Endocr Rev. 39, 1-20. doi: 10.1210/er.2017-00164.

Richards M, Nwadozi E, Pal S, Martinsson P, Kaakinen M, Gloger M, Sjöberg E, Koltowska K, Betsholtz C, Eklund L, Nordling S, Claesson-Welsh L (2022). Claudin5 protects the peripheral endothelial barrier in an organ and vessel-type-specific manner. Elife. 2022 11, e78517. doi: 10.7554/eLife.78517.

Rockey DC, Weymouth N, Shi Z. (2013). Smooth muscle α actin (Acta2) and myofibroblast function during hepatic wound healing. PLoS One. 8, e77166. doi: 10.1371/journal.pone.0077166.

Rotgers E, Jørgensen A, Yao HH-C (2018). At the crossroads of fate- somatic cell lineage specification in the fetal gonad. Endoc. Rev. 39, 739-759.

Sisk CL, Zehr JL. (2005). Pubertal hormones organize the adolescent brain and behavior. Front Neuroendocrinol. 26, 163-74. doi: 10.1016/j.yfrne.2005.10.003.

Sjöberg E, Meyrath M, Milde L, Herrera M, Lövrot J, Hägerstrand D, Frings O, Bartish M, Rolny C, Sonnhammer E, Chevigné A, Augsten M, Östman A. (2019). A Novel ACKR2-Dependent Role of Fibroblast-Derived CXCL14 in Epithelial-to-Mesenchymal Transition and Metastasis of Breast Cancer. Clin Cancer Res. 25, 3702-3717. doi: 10.1158/1078-0432.CCR-18-1294.

Sun C, Zhang K, Ni C, Wan J, Duan X, Lou X, Yao X, Li X, Wang M, Gu Z, Yang P, Li Z, Qin Z. (2023). Transgelin promotes lung cancer progression via activation of cancer-associated fibroblasts with enhanced IL-6 release. Oncogenesis 12, 18. doi: 10.1038/s41389-023-00463-5.

Templin JS, Wyrosdic JC, David CD, Wyrosdic BN, Lapp HE, Bala A, Bartlett A, Khan Z, Rokicki A, Park JH. (2019). Peripubertal gonadal steroids are necessary for steroid-independent male sexual behavior in castrated B6D2F1 male mice. Horm Behav. 113, 38-46. doi: 10.1016/j.yhbeh.2019.04.013.

Trova S, Bovetti S, Bonzano S, De Marchis S, Peretto P. (2021). Sex Steroids and the Shaping of the Peripubertal Brain: The Sexual-Dimorphic Set-Up of Adult Neurogenesis. Int J Mol Sci. 22, 7984. doi: 10.3390/ijms22157984.

Tsuji-Tamura K, Morino-Koga S, Suzuki S, Ogawa M. (2021). The canonical smooth muscle cell marker TAGLN is present in endothelial cells and is involved in angiogenesis. J Cell Sci. 134, jcs254920. doi: 10.1242/jcs.254920.

Viuff MH, Just J, Brun S, Dam TV, Hansen M, Melgaard L, Hougaard DM, Lappe M, Gravholt CH (2022). Women With Turner Syndrome Are Both Estrogen and Androgen Deficient: The Impact of Hormone Replacement Therapy. J Clin Endocrinol Metab. 107, 1983-1993. doi: 10.1210/clinem/dgac167.

Walters KA, Rodriguez Paris V, Aflatounian A, Handelsman DJ (2019). Androgens and ovarian function: translation from basic discovery research to clinical impact. J Endocrinol. 242, R23-R50. doi: 10.1530/JOE-19-0096.

Wang Y, Pan L, Moens CB, Appel B. (2014). Notch3 establishes brain vascular integrity by regulating pericyte number. Development 141, 307-17. doi: 10.1242/dev.096107.

Wang Y, Zhao Y, Chen S, Chen X, Zhang Y, Chen H, Liao Y, Zhang J, Wu D, Chu H, Huang H, Wu C, Huang S, Xu H, Jia B, Liu J, Feng B, Li Z, Qin D, Pei D, Cai J. (2022). Single cell atlas of developing mouse dental germs reveals populations of CD24+ and Plac8+ odontogenic cells. Sci Bull (Beijing) 67, 1154-1169. doi: 10.1016/j.scib.2022.03.012.

Xie T, Wang Y, Deng N, Huang G, Taghavifar F, Geng Y, Liu N, Kulur V, Yao C, Chen P, Liu Z, Stripp B, Tang J, Liang J, Noble PW, Jiang D. (2018). Single-Cell Deconvolution of Fibroblast Heterogeneity in Mouse Pulmonary Fibrosis. Cell Rep. 22, 3625-3640. doi: 10.1016/j.celrep.2018.03.010.

Young JM, McNeilly AS (2010). Theca: the forgotten cell of the ovarian follicle. Reproduction. 140, 489-504. doi: 10.1530/REP-10-0094.

Zhang K, Kagan D, DuBois W, Robinson R, Bliskovsky V, Vass WC, Zhang S, Mock BA. (2009). Mndal, a new interferon-inducible family member, is highly polymorphic, suppresses cell growth, and may modify plasmacytoma susceptibility. Blood 114, 2952-60. doi: 10.1182/blood-2009-01-198812.

Zheng W, Zhang H, Gorre N, Risal S, Shen Y, Liu K (2014a). Two classes of ovarian primordial follicles exhibit distinct developmental dynamics and physiological functions. Hum Mol Genet. 23, 920-28. doi: 10.1093/hmg/ddt486.

Zheng W, Zhang H, Liu K (2014b). The two classes of primordial follicles in the mouse ovary: their development, physiological functions and implications for future research. Mol Hum Reprod. 20, 286-292. doi: 10.1093/molehr/gau007.

Zhou Y, Zhu W, Guo Z, Zhao Y, Song Z, Xiao J (2007). Effects of maternal nuclear genome on the timing of puberty in mice offspring. J Endocrinol. 193, 405-12. doi: 10.1677/joe.1.07049.

Zhou Y, Zhou B, Pache L, Chang M, Khodabakhshi AH, Tanaseichuk O, Benner C, Chanda SK. (2019. Metascape provides a biologist-oriented resource for the analysis of systems-level datasets. Nat Commun. 10, 1523. doi: 10.1038/s41467-019-09234-6.

Zuckerman-Levin N, Frolova-Bishara T, Militianu D, Levin M, Aharon-Peretz J, Hochberg Z (2009). Androgen replacement therapy in Turner syndrome: a pilot study. J Clin Endocrinol Metab. 94, 4820-7. doi: 10.1210/jc.2009-0514.

Data availability

The scRNAseq data are in the process of deposition at the NIH GEO database.

ACKNOWLEDGEMENTS: We are grateful to Allison Pinder and Dr. Fredrick Tan for assisting with the genomic experiments and analyses. We thank Dr. Mamhud Siddiqi for his assistance with optical microscopy and image analyses. We thank Dr. Ru-Ching Hsia for helping with the electron microscopy experiments. We also thank the Carnegie Embryology supporting staff and the current and past Spradling lab members for their comments on the study, especially Haolong Zhu for assistance with scRNA-seq data analysis.

Funding: Howard Hughes Medical Institute

Author contributions:

Conceptualization: QY, ACS

Methodology: QY, ACS

Investigation: QY

Visualization: QY, ACS

Funding acquisition: ACS

Supervision: ACS

Writing – original draft: QY, ACS

Writing – review & editing: QY, ACS

Competing interests: None.

Supplementary Materials

Supplemental Methods

Figs. S1 to S6

Movies S1 to S10

Data S1 to S6

Fig. 1. Wave 1 follicles are remodeled prior to peri-puberty
(A). Schematic diagrams of fetal ovaries at indicated stages (above: E =embryonic day; P = postnatal day). Wave 1 follicles in the ovarian medulla (below dashed line) retain bipotential pregranulosa cells (BPGs) and develop without delay; epithelial pregranulosa cells (EPGs) replace BPGs on follicles in the cortex which become quiescent primordial follicles (wave 2).
(B) Postnatal follicular developmental timeline: wave 1 antral follicles: 2 weeks (Figure S1A-C); juvenile sexual development (peri-puberty): 4-5 weeks; puberty and ovulation: 7-8 weeks.
(C) Total follicles or wave 1 follicles (D) in P5 or P10 ovaries (see Figure 2A-D)
(E) Wave 1 ovarian volume vs age (mean +/- SD (bars); N=10)
(F) Wave 1 follicle remodeling (%) indicated by oocyte loss vs age (mean +/- SD (bars); N=3-4).

Fig. 2. Wave 1 follicles lose granulosa cells during remodeling
(A) Schematic diagram showing activation of Foxl2-EYFP expression initiated by Tamoxifen (Tx) injection leading to excision of a stop cassette EYFP expression (see Methods).
(B) Efficient EYFP labeling of granulosa cells in wave 1 medullar follicles of a 2 week ovary following Tx injection at E16.5 as shown in (A). Note virtual absence of labeling in cortical wave 2 follicles.
(C-D) Views of whole ovaries labeled as in A, and imaged at 2 week (C) or 5 week (D) and processed using Imaris to mark location of wave 1 follicles (balls).
(E) Wave 1 follicle numbers from Imaris analysis of (C-D).
(F) Section from a 5 week ovaries from (D) reveals ongoing remodeling of wave 1 follicles. Follicles near the medullar core are small (arrowheads), with few remaining EYFP-labeled granulosa cells, such as the follicle boxed in "1" (F'). A normal antral follicle "2" (F") with an oocyte contains many EYFP labeled granulosa cells. At right, the average number of EYFP-labeled GCs in medullar follicles prior to remodeling at 3 weeks is compared to the average number in remodeled medullar follicles at 5 weeks. Each point represents one analyzed follicle. **** $p<0.001$.
(G) A 6 week ovary after Tx injection at 5 week. A few central GCs in remodeled wave 1 follicles near the center of the image are labeled, showing they still express Foxl2 at 5 week.

Fig. 3. Follicles remodel to form an interconnected stromal network rich in thecal secretory cells.
(A) Schematic diagraming showing lineage labeling of Cyp17a1-epxressing thecal cells interstitial gland cells, and possibly other cells using Cyp17a1-iCre; CAG-tdTomato.
(B) 2 week ovary showing tdTomato-labeling of thecal cells sheathing follicles and putative interstitial gland cells between follicles.
(C) 3D reconstruction of follicles from with surrounding labeled thecal cells: Oocytes (green, DDX4), Cyp17a1-expressing cells (red). Scale bar, 20 µm.
(D-E) Whole mount staining of 2 week and 5 week ovary labeled, showing dramatic increase in labeled thecal, interstitial and possibly other Cyp17a1-lineage marked cells in the ovarian medulla.
(F-G) Oil red O staining (red color) reveals a significant increase in lipid droplet storage in ovarian medullar cells from 2 week (F) to 5 week (G) ovaries.

(H). Immunofluorescence staining of HSD3B1 and PLIN1 at 5 weeks shows that genes required for steroidogenesis and lipid droplet storage are highly expressed in medullar cells. Scale bar, 50 µm.
(I) Electron microscopy of remodeled thecal network showing cells with abundant lipid droplets (LD) and characteristic mitochondria (mt) (boxed region magnified in right panel).
(J) 3D reconstruction of an entire 5week ovary labeled by tdTomato expression activated by Cyp17a1-iCre.

Fig. 4. Single-cell RNA sequencing of 2 wk-6 wk ovaries
(A) UMAP plot of ovaries from 2 weeks to 6 weeks, showing 31 initial clusters (c0-c30). (A') the cell type groups indicated by colored regions as labeled and their relationship to the numbered initial clusters as shown in A.
(B) UMAP plot of re-clustered granulosa and epithelial cells from A showing 18 clusters (gc0-gc17) (B') the deduced ovarian follicle developmental stages labeled and indicated by colored regions and their relationship to the numbered clusters (numbers) shown in B.
(C) UMAP plot of re-clustered thecal, stromal and smooth muscle cells from A showing 21 clusters (gc0-gc20). (C') the deduced mesodermal cell subgroups labeled and indicated by colored regions and their relationship to the numbered clusters (numbers) shown in C.
(D) Diagram of steroidogenic genes in theca and granulosa cells giving rise to androgens such as testosterone and androstenedione, and their conversion in granulosa to estrogen.
(E) The estimated number of granulosa cells in follicles of the indicated developmental subclasses: primordial, primary, secondary, antral, remodeling, mitotic cycling.

Fig. 5. Model of wave 1 follicle development and function.
(A) Current model of follicle waves in juvenile mice (revised from 1A). Wave 1 follicles remodel to expand androgen-producing theca/interstitial cells during peri-puberty. A previously unrecognized "wave 1.5" consisting of primordial follicles located near the medullar/cortex border that were bound by both BPG and EPG cells, are activated starting at about 2 weeks, and generate normal follicles that account for the majority of mature follicles available at puberty.
(B) A diagram showing the deduced and proposed pathway of wave 1 follicle remodeling beginning at about 3 weeks. These steps are 1) oocyte (blue) loss; 2) loss of most granulosa cells (maroon); 3) expansion of steroidogenic, increase and interconnection of angiogenic and fibroblastic thecal cells (tan rectangles); 4) androgen biosynthesis and release contributing to normal juvenile development during peri-puberty, and support of new normal follicles (5 weeks).

Table 1. Summary of whole mount C57B ovary analyses.

Postnatal age	Total follicles/ ovary *	Antral *	Wave 1 *	Reference files	Ovaries analyzed
P5-7	3822 +/- 838	0	278 +/- 17	S1.mp4; S2.mp4	4
P10-P14	3304 +/- 926	0	293 +/- 36	S3.mp4; S4.mp4	3

3 wk	3089 +/- 669	23 +/- 2	ND	S5.mp4 S6.mp4	3
4 wk	ND	35 +/- 2	ND	S7.mp4 S8.mp4	4
5 wk	ND	24 +/- 4	ND	S9.mp4 S10.mp4	5

* numbers are mean and standard deviation

Fig. 1

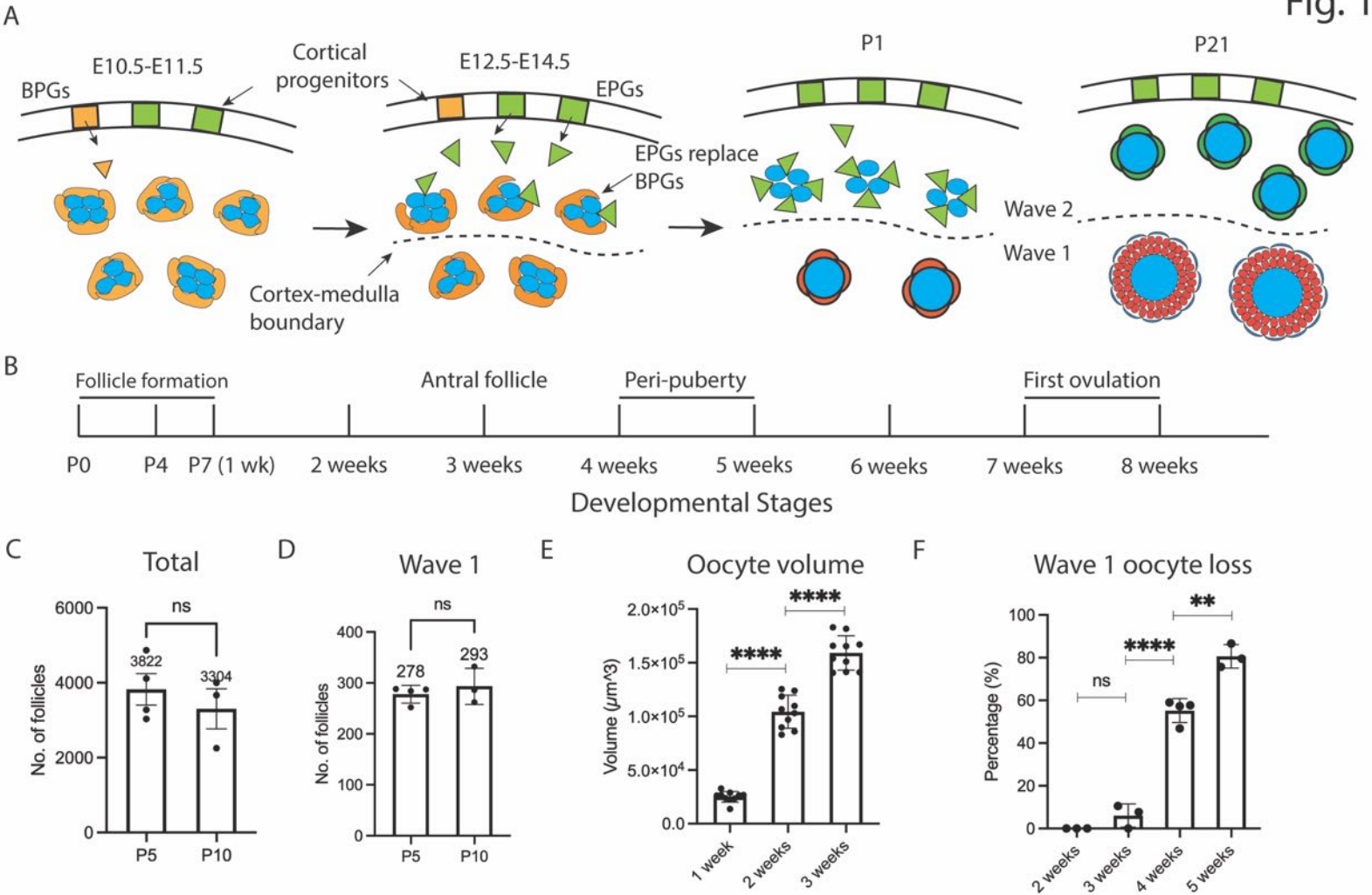
A
E10.5-E11.5
BPGs
Cortical progenitors
E12.5-E14.5
EPGs
EPGs replace BPGs
P1
P21
Wave 2
Wave 1
Cortex-medulla boundary
B
Follicle formation
Antral follicle
Peri-puberty
First ovulation
P0
P4
P7 (1 wk)
2 weeks
3 weeks
4 weeks
5 weeks
6 weeks
7 weeks
8 weeks
Developmental Stages
C
Total
No. of follicles
ns
3822
3304
P5
P10
D
Wave 1
No. of follicles
ns
278
293
P5
P10
E
Oocyte volume
Volume (μm^3)
****
****
1 week
2 weeks
3 weeks
F
Wave 1 oocyte loss
Percentage (%)
ns
****
**
2 weeks
3 weeks
4 weeks
5 weeks

Fig. 2

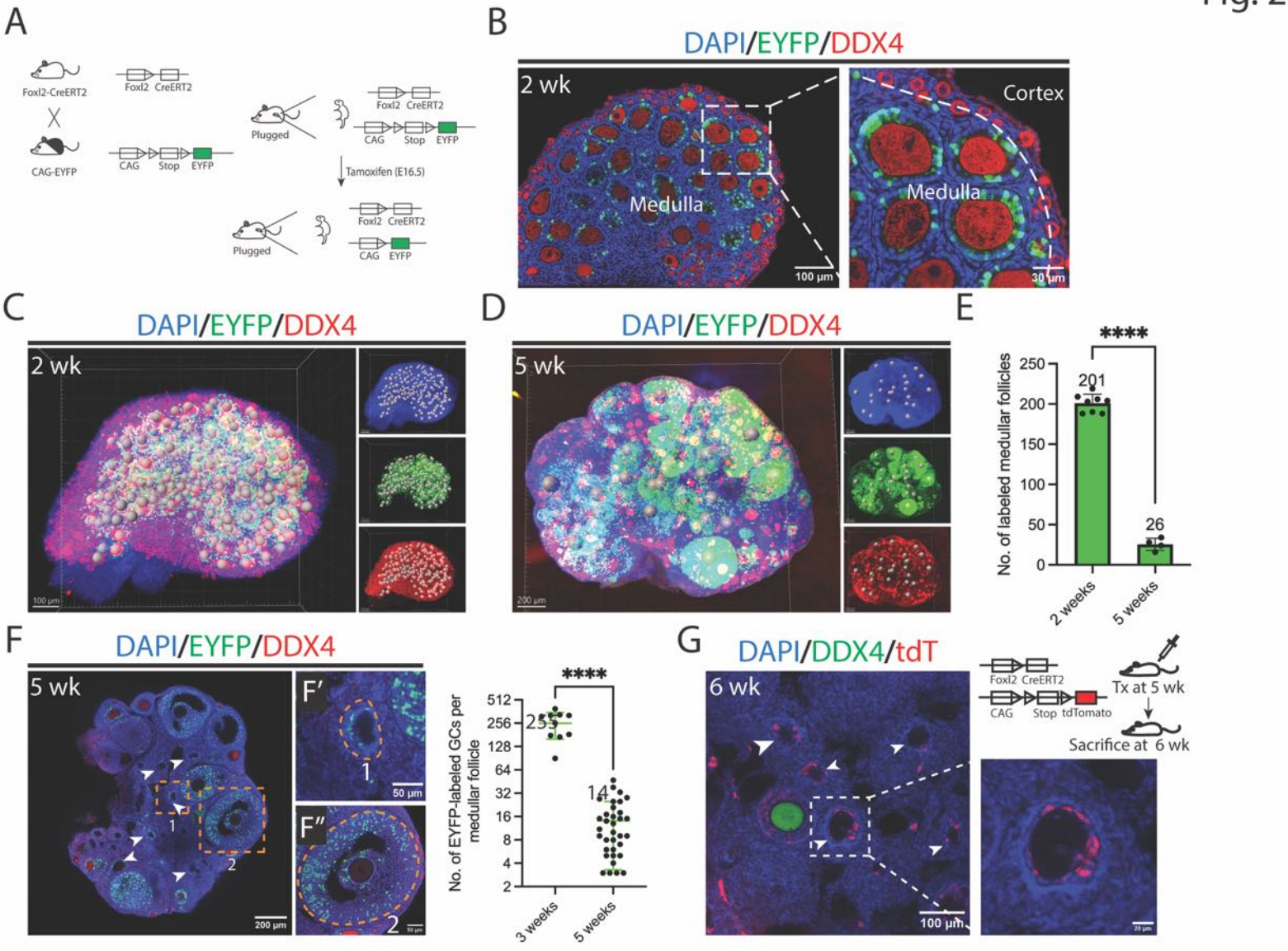
A
Foxl2-CreERT2
CAG-EYFP
Foxl2 CreERT2
CAG Stop EYFP
Plugged
Tamoxifen (E16.5)
B
DAPI/EYFP/DDX4
2 wk
Medulla
Cortex
100 µm
30 µm
C
DAPI/EYFP/DDX4
2 wk
D
DAPI/EYFP/DDX4
5 wk
E
****
No. of labeled medullar follicles
201
26
2 weeks
5 weeks
F
DAPI/EYFP/DDX4
5 wk
F′
F″
200 µm
50 µm
No. of EYFP-labeled GCs per medullar follicle
255
14
3 weeks
5 weeks
G
DAPI/DDX4/tdT
6 wk
Foxl2 CreERT2
CAG Stop tdTomato
Tx at 5 wk
Sacrifice at 6 wk
100 µm

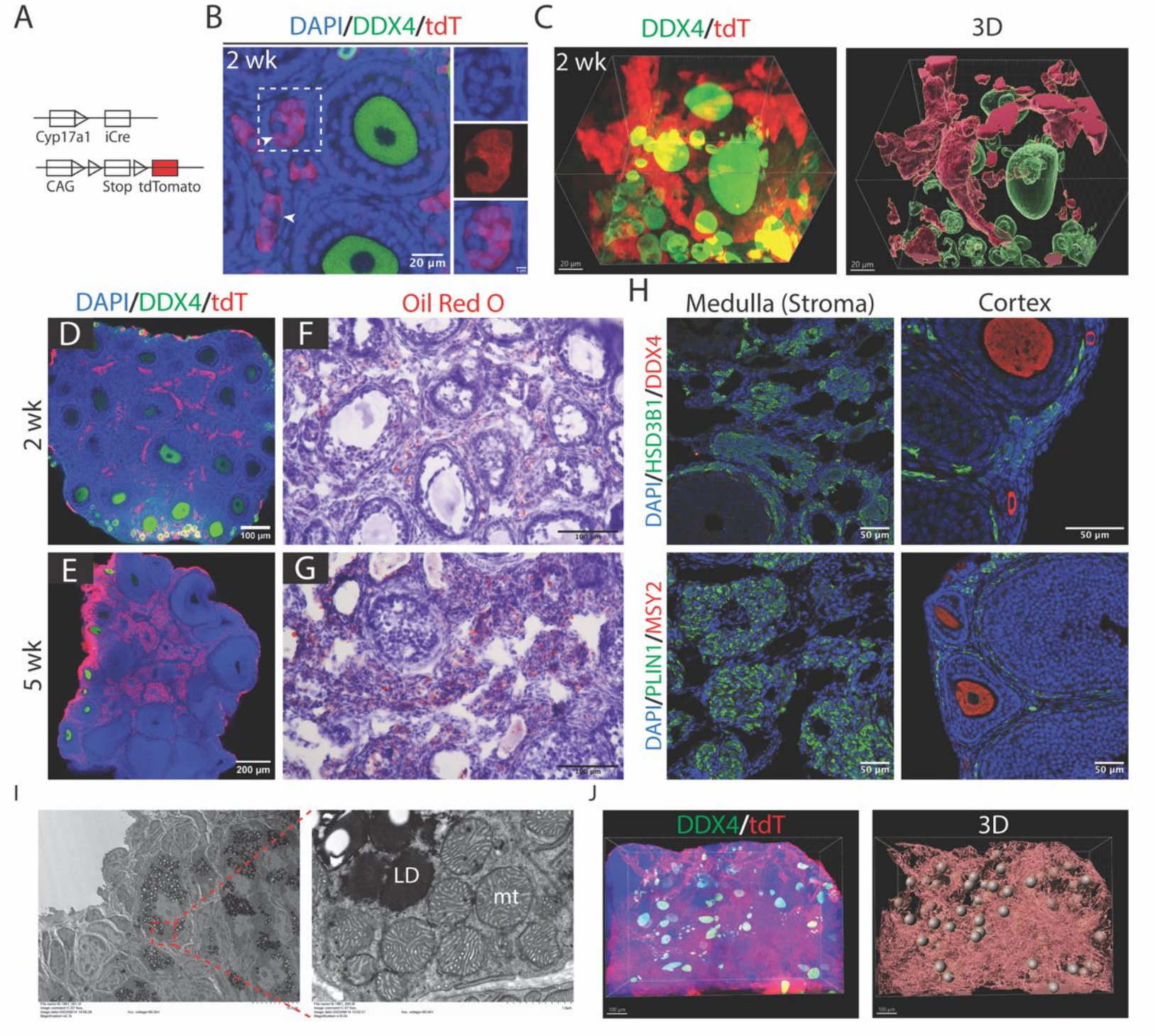
A
Cyp17a1
iCre
CAG
Stop
tdTomato
B
DAPI/DDX4/tdT
2 wk
20 µm
C
DDX4/tdT
2 wk
20 µm
3D
20 µm
DAPI/DDX4/tdT
Oil Red O
D
F
2 wk
100 µm
100 µm
E
G
5 wk
200 µm
100 µm
H
Medulla (Stroma)
Cortex
DAPI/HSD3B1/DDX4
DAPI/PLIN1/MSY2
50 µm
50 µm
50 µm
50 µm
I
LD
mt
J
DDX4/tdT
3D

Fig. 4

A

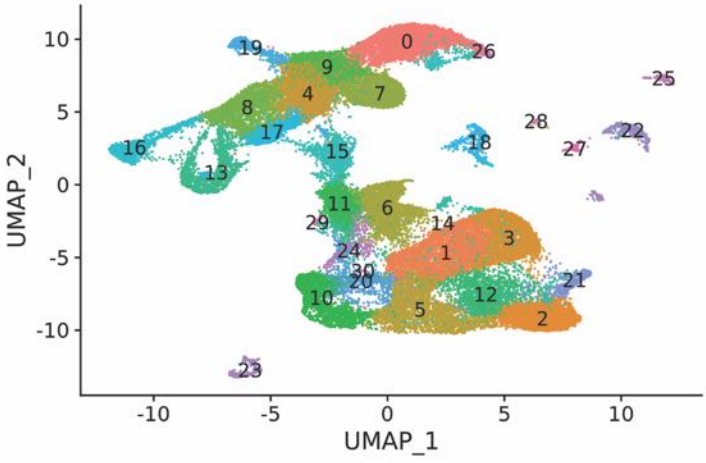

A′

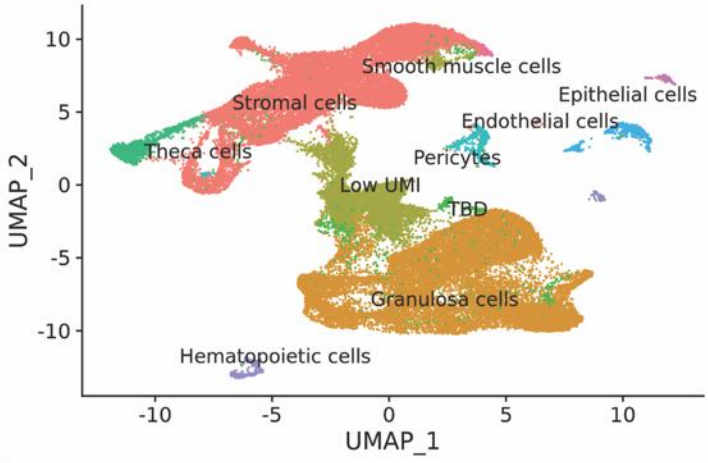

B

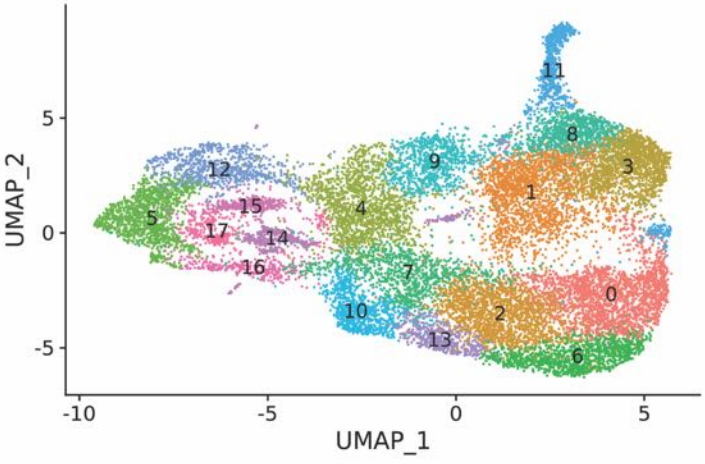

B′

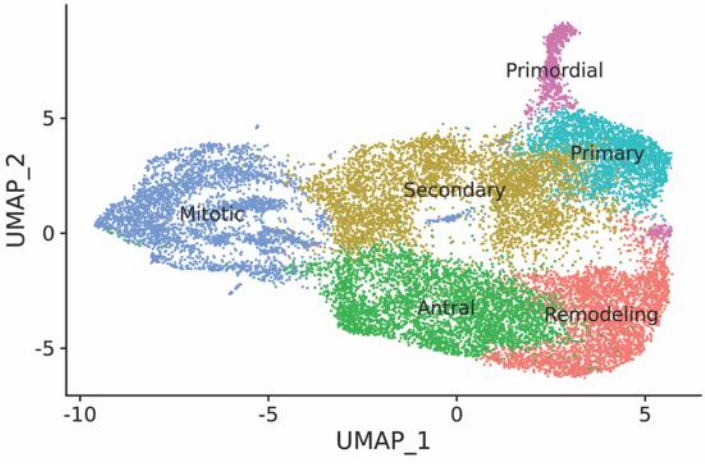

C

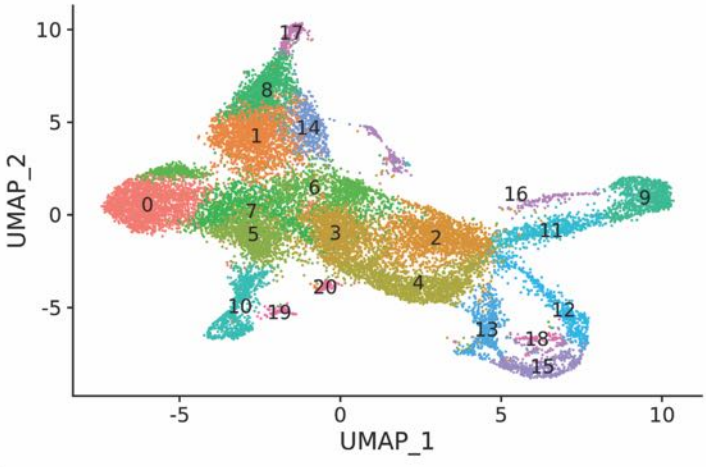

C′

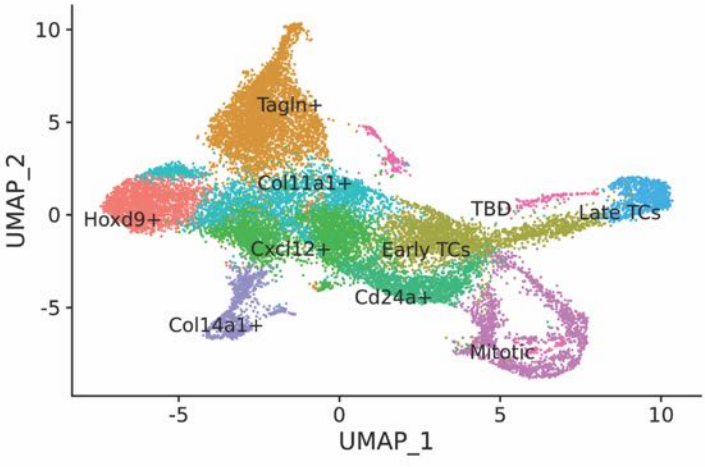

D

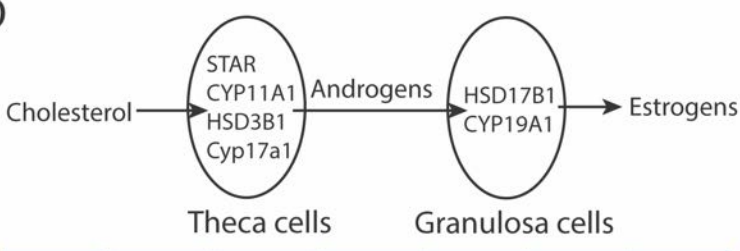

		2 wk (9471)	3 wk (9253)	4 wk (11077)	5 wk (7779)	6 wk (10583)
Theca cells	Cyp11a1 &Hsd3b1 &Cyp17a1	96	75	147	633	89
	Cyp11a1 &Hsd3b1 &Cyp17a1 &Star	41 (42.7%)	32 (42.7%)	72 (49.0%)	526 (83.1%)	29 (32.6%)
Granulosa cells	Hsd3b1 &Hsd17b1 &Cyp19a1	247	202	68	238	626

E

	2 wk	3 wk	4 wk	5 wk	6 wk
Primordial	316	206	124	81	81
Primary	794	742	392	230	365
Secondary	1086	1131	896	442	760
Antral	356	587	1416	590	1050
Remodeling	77	138	1348	766	910
Mitotic cycling	478	647	1072	620	749

Fig. 5

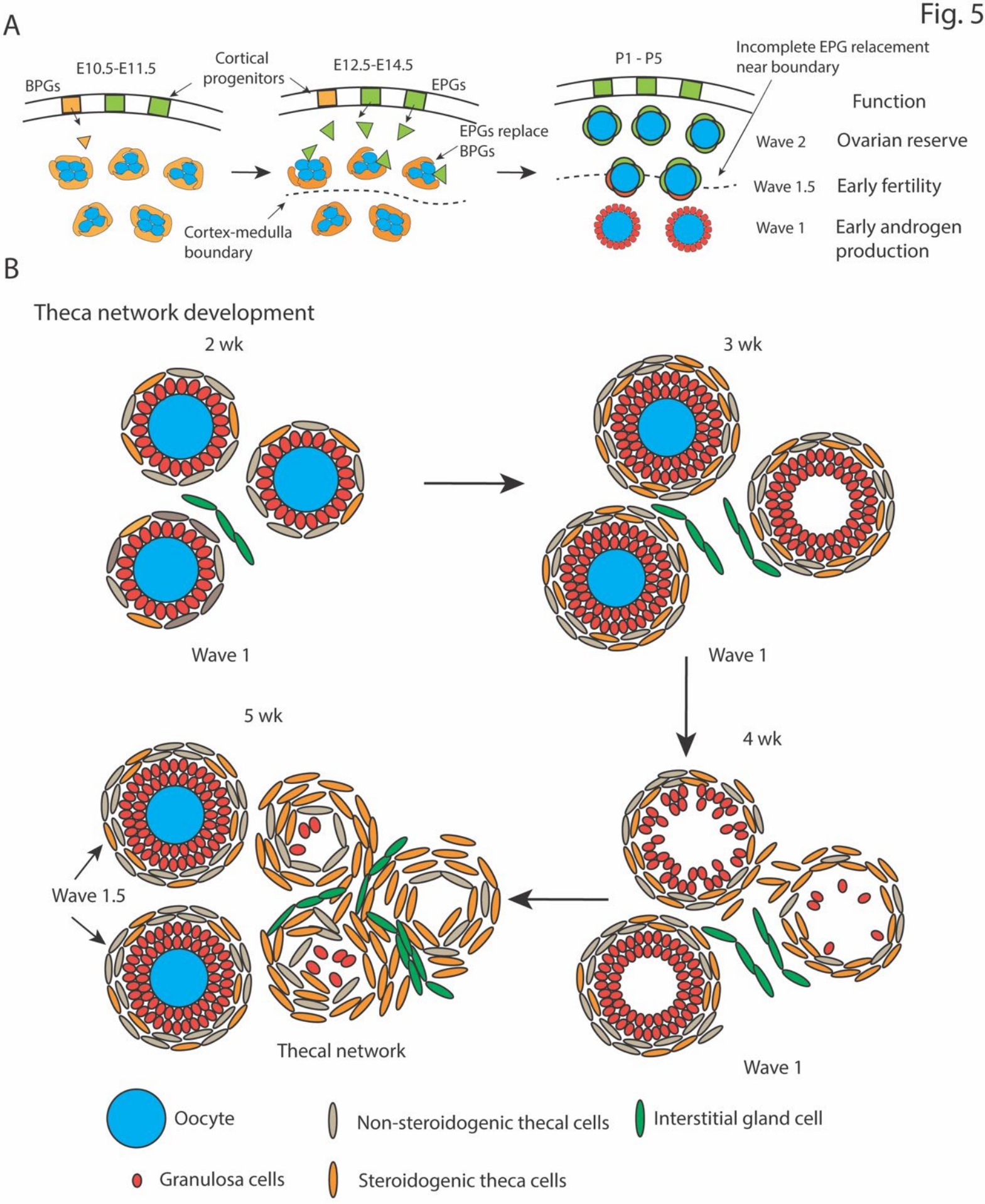
A
E10.5-E11.5
BPGs
Cortical progenitors
E12.5-E14.5
EPGs
EPGs replace BPGs
Cortex-medulla boundary
P1 - P5
Incomplete EPG relacement near boundary
Function
Wave 2
Ovarian reserve
Wave 1.5
Early fertility
Wave 1
Early androgen production
B
Theca network development
2 wk
Wave 1
3 wk
Wave 1
4 wk
Wave 1
5 wk
Wave 1.5
Thecal network
Oocyte
Non-steroidogenic thecal cells
Interstitial gland cell
Granulosa cells
Steroidogenic theca cells

Supplementary Materials

MATERIALS AND METHODS

Experimental mice

All animal experiments were conducted in compliance with the Institutional Animal Care and Use Committee guidelines of the Carnegie Institution of Washington. The mice were housed in specific pathogen-free facilities at CIW. The strains of mice used in the study included B6;129P2-Foxl2tm1 mice (GFP/cre/ERT2)Pzg/J (referred to as Foxl2-CreERT2 in the paper, Strain #: 015854), STOCK XO/J (XO mice, Strain #: 036414), B6.129X1-Gt(ROSA)26Sortm1(EYFP)Cos/J (R26R-EYFP, Strain #: 006148), and B6;SJL-Tg(Cyp17a1-icre)AJako/J (Cyp17icre, Strain #: 028547). The R26R-tdTomato mice were generously provided by Chen-Ming Fan at the Carnegie Institution for Science.

Lineage tracing experiments

To visualize the expression patterns of Foxl2 and Cyp17a1, we generated reporter mouse lines by crossing R26R-EYFP or R26R-tdTomato mice with Foxl2-CreERT2 or Cyp17a1-iCre (Shimshek et al. 2002) mice. The presence of a vaginal plug was designated as embryonic day 0.5 (E0.5), and pregnant females were injected with 1 mg tamoxifen per 35 g body weight at E16.5 (Foxl2-CreERT2). We collected gonads from fetuses or ovaries from pups at the indicated stages for analysis.

To investigate the expression of Foxl2 in remodeling follicles, Tamoxifen was injected at a concentration of 1 mg/35 g into female mice at 5 wks of age. The ovaries were dissected one wk later and subjected to whole mount staining for analysis as before.

Immunostaining

For whole mount staining, gonads or ovaries were first fixed in 4% PFA overnight at 4°C. The tissues were then washed three times in a washing buffer containing 0.3% Triton-100 and 0.5% Thioglycerol in DPBS, and incubated in blocking buffer (1% Normal donkey serum, 1% BSA and 0.3% Triton-100 in DPBS) overnight at 37°C. Primary antibodies were then added to the dilution buffer (1% BSA and the 0.3% Triton-100 in DPBS) and the samples were incubated for two days at 37°C. After washing in the washing buffer overnight at 37°C, the secondary antibodies were applied and incubated for another two days at 37°C, followed by washing in the washing buffer with DAPI overnight at 37°C. To increase opacity, the clearing buffer Ce3D (containing 4g Histodenz in 2.75 ml 40% (v/v) N-methylacetamide) was then applied. Finally, the samples were imaged using an inverted SP8 and Inverted STELLARIS 8 microscope. Images were analyzed using Fiji or Imaris.

For cryosection staining, the dissected tissues were fixed in 4% PFA overnight at 4°C. After washing three times in DPBS, the tissues were dehydrated sequentially in 10% and 30% sucrose solutions and embedded in O.C.T. for cryosectioning. After treating with 0.01% sodium citrate buffer to retrieve the antigens, the slides were blocked for 1 h at room temperature, incubated with primary antibodies overnight at 4°C, and secondary antibodies and DAPI for 1h at room temperature. The samples were then imaged with an upright SP5 microscope, and the images were analyzed using Fiji.

Oil Red O Staining

Oil Red O Staining was performed according to the protocol provided by abcam (ab150678). Briefly, the slides were placed in Propylene Glycol for 5 minutes at room temperature, followed

by incubation in Oil Red O solution at 60°C for 6-10 minutes. The slides were then differentiated in 85% Propylene Glycol for 1 minute. After rinsing twice in distilled water, the slides were incubated in Hematoxylin for 1 minute, then rinsed thoroughly in tap water and twice in distilled water. The slides were ready for imaging after applying a coverslip using an aqueous mounting medium. Imaging was done using a Nikon Eclipse E800 microscope.

Genotyping

The tissue was cut and placed in a lysis buffer (30 mM Tris-HCl, 0.5% Triton X-100, 20 µg/mL Proteinase K) and incubated at 50°C overnight. The proteinase K was then inactivated by heating the sample to 95°C for 5 minutes. For genotyping using general PCR, 1 µL of the sample was added to the PCR mixture. For quantitative PCR (qPCR), primers and probes were designed to amplify and detect the target DNA sequence from both the X chromosome and an autosome. The amount of amplification from the X chromosome was compared to the amount from the autosome to determine the genotype, specifically whether the sample is XO or has two X chromosomes. The qPCR was performed in a CFX 96 Real-Time PCR machine.

Single cell RNA sequencing

Tissue samples were first dissected in PBS, and then digested using 0.25% Trypsin/EDTA at 37°C for approximately 20 minutes. The digestion was stopped by adding 10% FBS, and the resulting cell suspension was filtered through a 100 µm strainer to remove any remaining undissociated structures. The cells were then collected by centrifugation and suspended in PBS containing 0.04% BSA. Samples with a viability of over 90% were selected for subsequent sequencing. Libraries of the single cells were prepared using the Chromium Next GEM Single Cell 3' Reagent Kits v3.1 from 10X Genomics, with the goal of capturing 10,000 cells per sample. The sequencing was performed using the Nextseq 500 platform from Illumina according to 10XGenomics recommendations of: paired-end, single index reads with Read 1 being 28 cycles, Index 1 being 8 cycles, and Read 2 being 91 cycles. Sequencing was to a depth of 50,000 reads per cell.

The single-cell sequencing datasets were initially processed using the Cell Ranger pipeline (v3.1.0 and v6.0.1) with default settings. Further analysis of the scRNA-seq data was performed using the Seurat package (v4.1.0). The count data were read and transformed into a Seurat object using the Read10X and CreateSeuratObject functions. The library (2 wks, 3 wks, 4 wks, 5 wks, and 6 wks) were preprocessed with NormalizeData(), followed by FindVariableFeatures(), FindIntegrationAnchors(), and IntegrateData() using default settings.

The integrated object was further processed using ScaleData(), RunPCA(npcs = 50), RunUMAP(dims = 1:30), FindNeighbors(dims = 1:30), FindClusters(resolution = 1.0), and RunTSNE(dims = 1:30) with other default settings to determine cell clusters. Further clustering of granulosa cells and mesenchymal cells was performed using subset(), followed by the cell clustering methods mentioned above

The electron microscope

Mice ovaries were excised and fixed in a solution of 2% paraformaldehyde, 2.5% glutaraldehyde, in 0.1 M PIPES buffer (pH 7) at 4°C overnight. The ovaries then were washed and treated with 50mM glycine in 0.1 M PIPES buffer for 15 minutes, followed by washing with 0.1M PIPES buffer. Tissue pieces were then postfixed with 1% osmium tetroxide, 1.5% potassium ferrocyanide in 0.1 M PIPES buffer for 60 min, washed with water and en bloc staining with 1% (w/v) uranyl acetate for 60 min. Following, the ovaries were serial dehydrated using graded ethanol solutions, including 30%, 50%, 75%, 85%, 95% and 100% ethanol and

two exchanges of 100% acetone. After dehydration, the ovaries were infiltrated and embedded in EmBed 812 Epoxy resin (Electron Microscopy Sciences, PA) following manufacturer's recommendation. Ultrathin sections at ~70 nm thickness were cut on a Leica EMUC7 ultramicrotome (Leica Microsystems, Inc., Bannockburn, IL), and examined in a Hitachi HT7800 transmission electron microscope operated at 80KeV. Digital images were acquired by using an AMT NanoSprint 12 camera.

Statistical analysis

The data are reported as means ± SD of biological replicates, and no statistical methods were used to determine the sample size. Differences between two groups were compared using a two-tailed Student's t-test. $P < 0.05$ was considered statistically significant.

Supplemental Figures

Fig. S1. Wave 1 follicle development in the early juvenile ovary.

(A-D) Wave 1 follicles stained for DDX4 (green) at P5, P7, P14 (2 week) and P21 (3 weeks). Based on cell morphology (arrow) theca cells are already forming at P5 (A). The follicles go through to late primary at P7 with more granulosa cells in one layer (B), to secondary follicle at P14 with several layers of granulosa cells (C) and to antral follicles at P21 with the oocyte forming non-surrounded nucleus (D).

(E-F') Quantification of wave 1 (E-F) and total (E'-F') follicles throughout the ovary using Ce3D and Imaris software (gray balls). The follicles with oocytes >20 µm in diameter (located mostly in medulla) are considered to be wave 1 follicles; all DDX4 positive cells counted manually were used to define total follicles.

(G-G') Whole mount staining and 3D reconstruction of ovary at P14. A surface model generated using Imaris software defines the oocyte boundaries, excluding the nucleus.

Fig. S2. Wave 1 follicles begin to remodel by 3 wks.

(A) C57BL/6J ovaries stained for DDX4 (green) and DAPI showing extensive remodeling (formerly termed "atresia") of wave 1 follicles (arrowheads). Some normal developing follicles are present(arrows) that probably represent follicles activated after wave 1. Left (4 weeks): Oocyte become distorted, and granulosa cells are reduced in number and no longer form well-organized layers. Right (5 weeks): Boundaries between former follicles become indistinct and holes left by the degenerated nuclei shrink in size but are still visible.

(B) DAPI-stained DBA/2J ovaries showing wave 1 follicle remodeling (arrowheads) and normal developing follicles (arrows). Left (3 weeks): Early remodeling follicles are found in the central medulla. Right (7 weeks): wave 1 derivatives that still retain holes remain visible (arrowheads) along with normal follicles (arrows) and corpus lutei (asterisks).

(C) Electron microscopy of wave 1 follicles. In a normal follicle, the oocyte is closely intact with the zona pellucida (ZP) and even granulosa cells through microvilli. In a remodeling intermediate follicle, the cytoplasm of the oocyte shrinks, as indicated by the space between the oocyte and ZP, and the absence of microvilli on the ZP. In a fully remodeling follicle, the oocyte disappears, while the ZP persists; the thecal cells and related interstitial gland cells further accumulate lipid droplets. Oo: Oocyte; ZP: Zona pellucida; LD: Lipid droplet; mt: Mitochondria.

Fig. S3. Lineage tracing wave 1 granulosa cells
(A-D) Lineage labeling using Foxl2-CreERT2 and CAG-tdTomato. Tamoxifen was administrated at E16.5. (B) Control experiment to rule out EGFP expression from the Foxl2-EGFP-CreRT2 construct contributes to apparent EYFP granulosa cell labeling in Figure 2 and Figure S3D-J). Note that EGFP expression from Foxl2-EGFP-CreRT2 is very low, and its expression pattern (cytoplasmic only, differs from the strong cytoplasm and nuclear expression of EYFP after stop sequence removal). At 2 weeks, many small primordial follicles located near the cortex-medulla border are partially labeled (examples shown in C) in addition to large wave 1 follicles lin the medulla. By 5 weeks, wave 1 follicles have remodeled, while large follicles contain granulosa cells mosaic for Tomato expression, fully recapitulating the previous results with EYFP. These intact large follicles, most likely derived from wave 1.5 progenitors. Arrowhead: remodeled wave 1 follicle; arrow: large follicle with mosaic tdTomato expression. Primary follicle (enlarged in D), showing that EGFP expression from Foxl2-EGFP-CreRT2 is confined to the cell cytoplasm, unlike the expression observed in previous experiments using activated EYFP expression.
(E-I) Lineage labeling using Foxl2-CreERT2 and CAG-EYFP. At 2 weeks, one or more granulosa cells (E) in some primordial follicles are labeled by EYFP enlarged in "1", "2", "3"). (F) Counts showed that 7% (421+/-74) of 5,843+/-1256 total primordial follicles contained EYFP-labeled granulosa cells (E, see also Fig. 1D). (G) 80% of remodeled follicles still contain some EYFP-labeled granulosa cells at 5 weeks, consistent with their wave 1 origin. Dashed line: contour of follicle; arrowheads: EYFP-positive granulosa cells.
(H) About 70% of secondary follicles in 5 week ovaries, also contain EYFP-labeled granulosa cells suggesting that they also derive from activated wave 1.5 follicles.
(I) After lineage labeling ovarian cells at E16.5 (Figure 2E), >90% of wave 1 follicles have EYFP-positive granulosa cells at 2weeks. At 5wks > 70% of normal antral follicles (Total 37) contain EYFP-positive granulosa cells, even though >80% of wave 1 follicles have lost oocytes and remodeled (Figure 1F).

Fig. S4. Expansion of theca cells and its related cells - interstitial gland population.
(A) Immunofluorescence staining of CYP19A1 in the ovary at 3 weeks and 5 weeks. Significant increase of theca cells and interstitial gland is observed at stroma from 3 weeks to 5 weeks.
(B-C) Immunofluorescence staining of Cyp17a1 lineage-traced ovary at 2 weeks. Initially, expression was observed in theca cells and associated cells that appear to be interstitial gland cells (arrows). In addition, a few granulosa cells were labeled (arrowheads), as reported before (Bridges et al., 2008).
(D) Cyp17a1 lineage-traced ovary at 4 weeks and 7 weeks. A significant increase in the number of labeled theca cells and interstitial gland cells is observed at 7 weeks compared to 4 weeks. In this staining, the signals from labeled theca cells and interstitial gland cells are much brighter than those from granulosa cells. This is likely because the tdTomato antibody has more difficulty penetrating the follicle to reach granulosa cells compared to the theca cells and interstitial gland cells. (E) Structurally, steroidogenic theca cells closely resemble interstitial cells. In the image, red lines are used to distinguish zones enriched in interstitial cells (1), theca cells (2), and granulosa cells (3). The rectangle labeled "1" indicates interstitial cells, while the

rectangle labeled "2" represents steroidogenic theca cells, and the rectangle labeled "3" indicates granulosa cells. nu: Nucleus. LD: Lipid droplet; mt: Mitochondria.

Fig. S5. Analysis of single-cell RNA sequencing
(A) The ovarian cells from 2 to 6 weeks contribute to almost every cluster in the UMAP plot.
(B) Summary of marker gene expression in cell clusters, including granulosa cells, stromal cells, theca cells, epithelial cells, smooth muscle cells, endothelial cells, pericytes, hematopoietic cells, TBD (to be determined) cells, and cells with low UMI or higher mitochondrial content.
(C) The marker gene expression for granulosa cells from different stages of follicles, including primordial follicle, primary follicle, secondary follicle, antral follicle, remodeling follicle, and cells in mitotic cycles.
(D) The marker gene expression for the reanalysis of mesenchymal cells, including stromal theca cells expressing Cyp17a1, Tagln+ fibroblasts, Col14a1+ fibroblasts, Cd24a+ fibroblasts, Cxcl14+ fibroblasts, Hox9+ fibroblasts, and mitotic cells expressing Mki67.

Fig. S6. Hormone receptor expression and XO mouse line.
(A) Androgen receptor is expressed in almost all cell types, while estrogen receptor 1 (Esr1) is expressed in theca cells, epithelial cells, and smooth muscle cells and Estrogen receptor 2 (Esr2) is expressed in granulosa cells and some TBD cells. No follicle-stimulating hormone receptor (Fshr) is expressed, and luteinizing hormone/choriogonadotropin receptor (Lhcgr) is expressed in theca cells.
(B) The total number of follicles in XO mice is significantly less than in control XX mice.
(C) Activated follicles (normally wave 1 follicles, but not so in XO mice) in XO mice are much less than activated follicles in XX mice at P7, but are replenished by some wave 2 or wave 1.5 follicles by 2 weeks, as there is no statistical difference between XO and XX at 2 weeks.

Table S1. Antibodies

Name	Source	Identifier	Dilution
Anti-EGFP (Chicken)	Aves labs	GFP-1020	1:300
Anti-DDX4 (Rabbit)	Abcam	ab13840	1:300
Anti-MSY2 (Mouse)	Abcam	sc-393840	1:100
Anti-tdTomato (Goat)	Origene Tech	AB8181-200	1:300
Anti-HSD3B1 (Mouse)	Santa Cruz	sc-515120	1:100
Anti-Cyp17a1 (Rabbit)	Cell Signaling Technology	94004T	1:100
Anti-PLIN1	abcam	ab3526	1:100

DAPI	Sigma	D9542-10mg	0.5ug/ml
Alexa Fluor® 488 AffiniPure™ Donkey Anti-Chicken IgY (IgG) (H+L)	Jacksonimmuno	703-545-155	1:300
Alexa Fluor® 594 AffiniPure™ Donkey Anti-Goat IgG (H+L)	Jacksonimmuno	705-585-147	1:300
Alexa Fluor 488 donkey anti-mouse lgG	invitrogen	A21202	1:300
Alexa Fluor 568 donkey anti-mouse lgG	invitrogen	A10037	1:300
Alexa Fluor 488 donkey anti-mouse lgG	invitrogen	A21206	1:300
Alexa Fluor 568 donkey anti-rabbit lgG	invitrogen	A10042	1:300
Alexa Fluor 647 donkey anti-rabbit lgG	invitrogen	A31573	1:300

Table S2. Primers

Name	Forward (5'-3')	Reverse (5'-3')	Size	Chromosome	Note
XO-qPCR-Tg	GACTAGGTTCATAGGCACTGG	CCGCCAAAACTCCTTCTCTAC	123 bp	X	Genotyping for XO mice
XO-qPCR-Tg-Probe	[5HEX]CCCCAGATGGTACCCACAGAACTTG			X	
XO-qPCR-IPC	CACGTGGGCTCCAGCATT	TCACCAGTCATTTCTGCCTTTG	74 bp	12	
XO-qPCR-IPC-Probe	[Cy5]CCAATGGTCGGGCACTGCTCAA			12	
Foxl2-Mutant	AGAGAAGAGAGTGAGAGCCG	GTCCAGCTCGACCAGGATGG	221 bp	9	Genotyping for Foxl2-CreERT2
Foxl2-WT	AGAGAAGAGAGTGAGAGCCG	GAGCGCCACGTACGAGTACG	335 bp	9	
Cyp17a1-Tg	GCTGTAGCTTCTCCACTCCAC	CAGGTTTTGGTGCACAGTCA	120 bp		Genotyping for Cyp17a1-iCre
Cyp17a1-IPC	AGTGGCCTCTTCCAGAAATG	TGCGACTGTGTCTGATTTCC	521 bp		

Supplementary Data

S1 scRNAseq_2-6wk
S2_Initial cluster gene expression_c0-c30
S3 Reclustered granulosa gene expression_gc0-gc17
S4_Reclustered mesenchymal gene expression. g0-g20.

S5 Up to 250 preferentially expressed genes from each cluster
S6 Cell number associated with each cluster

Fig. S1

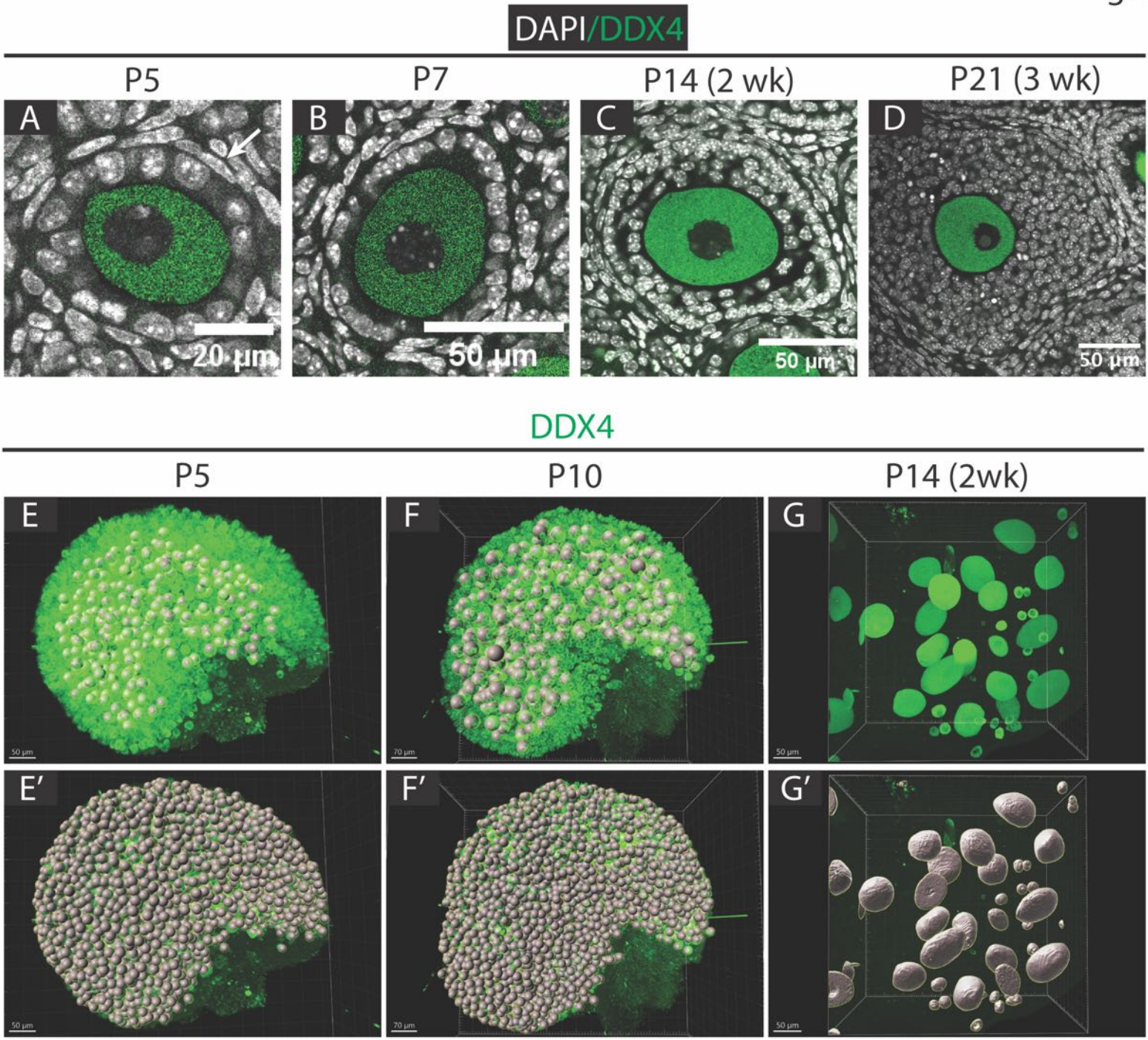
DAPI/DDX4
P5
P7
P14 (2 wk)
P21 (3 wk)
A
B
C
D
20 µm
50 µm
50 µm
50 µm
DDX4
P5
P10
P14 (2wk)
E
F
G
E′
F′
G′
50 µm
70 µm
50 µm
50 µm
70 µm
50 µm

Fig. S2

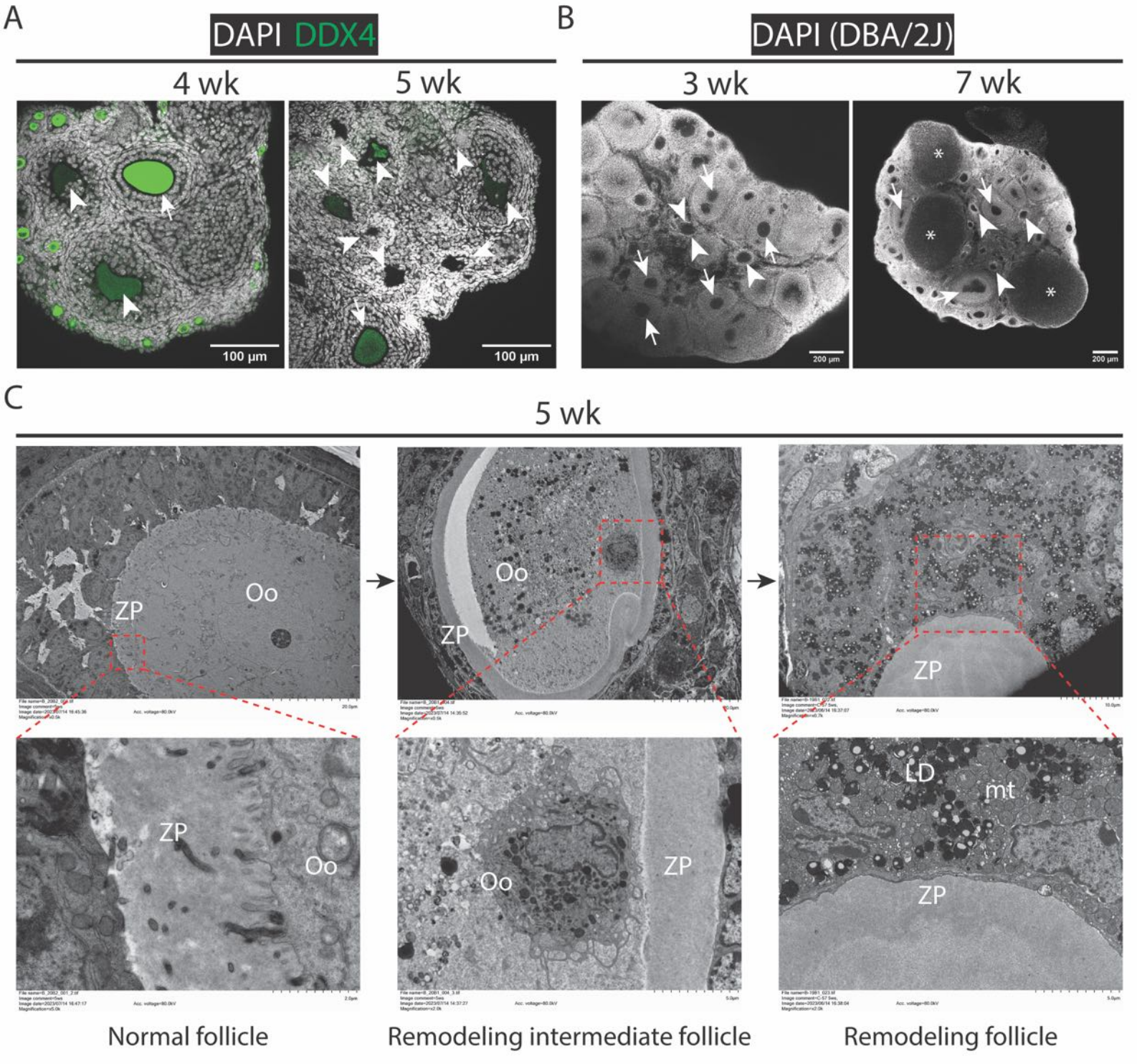
A
DAPI DDX4
4 wk
5 wk
100 μm
100 μm
B
DAPI (DBA/2J)
3 wk
7 wk
200 μm
200 μm
C
5 wk
ZP
Oo
ZP
Oo
ZP
ZP
Oo
ZP
Oo
ZP
LD
mt
ZP
Normal follicle
Remodeling intermediate follicle
Remodeling follicle

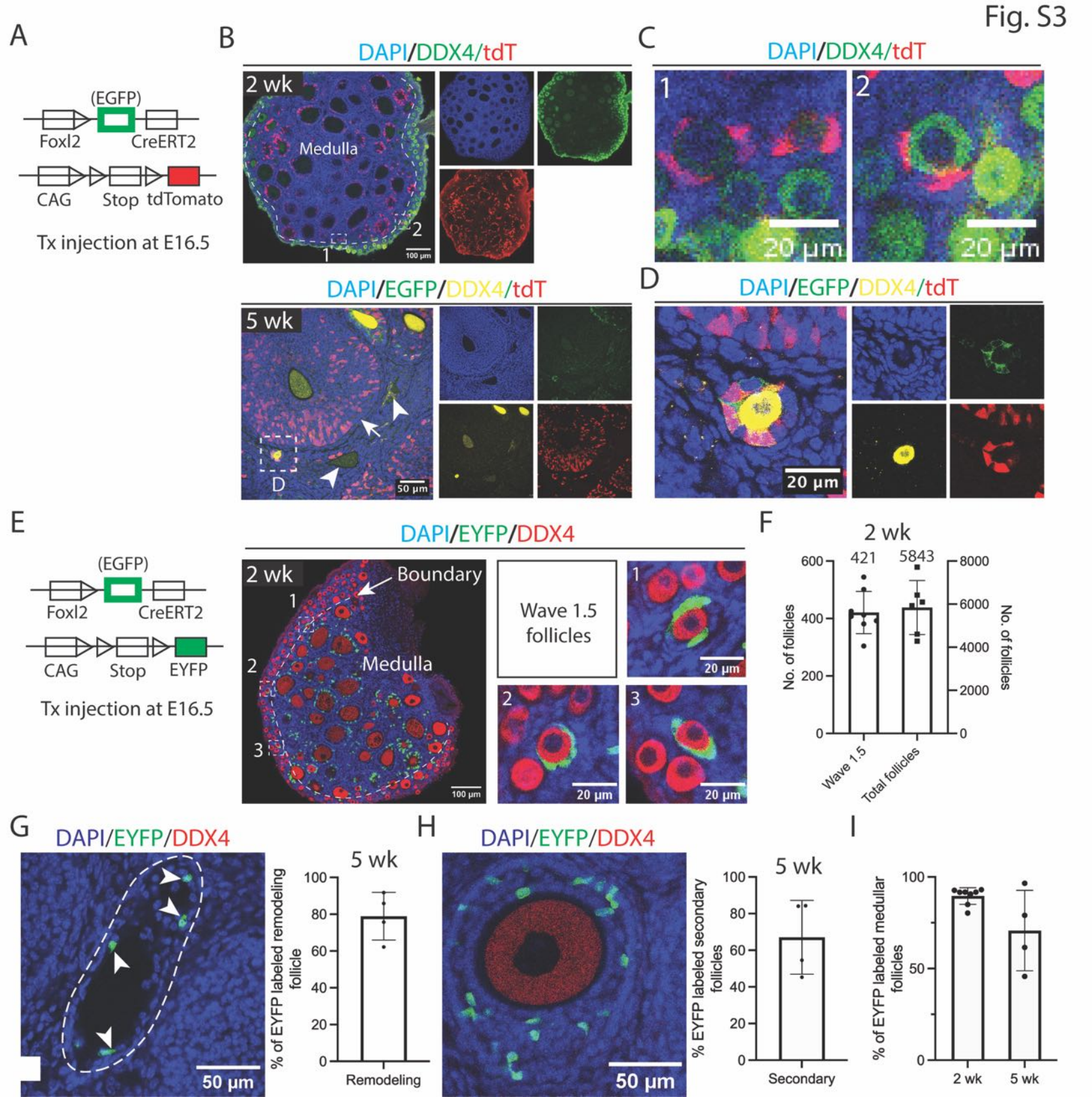
Fig. S3
A
(EGFP)
Foxl2
CreERT2
CAG
Stop
tdTomato
Tx injection at E16.5
B
DAPI/DDX4/tdT
2 wk
Medulla
1
2
100 µm
DAPI/EGFP/DDX4/tdT
5 wk
D
50 µm
C
DAPI/DDX4/tdT
1
2
20 µm
20 µm
D
DAPI/EGFP/DDX4/tdT
20 µm
E
(EGFP)
Foxl2
CreERT2
CAG
Stop
EYFP
Tx injection at E16.5
DAPI/EYFP/DDX4
2 wk
Boundary
1
2
3
Medulla
100 µm
Wave 1.5 follicles
1
2
3
20 µm
20 µm
20 µm
F
2 wk
421
5843
No. of follicles
No. of follicles
Wave 1.5
Total follicles
G
DAPI/EYFP/DDX4
50 µm
5 wk
% of EYFP labeled remodeling follicle
Remodeling
H
DAPI/EYFP/DDX4
50 µm
5 wk
% EYFP labeled secondary follicles
Secondary
I
% of EYFP labeled medullar follicles
2 wk
5 wk

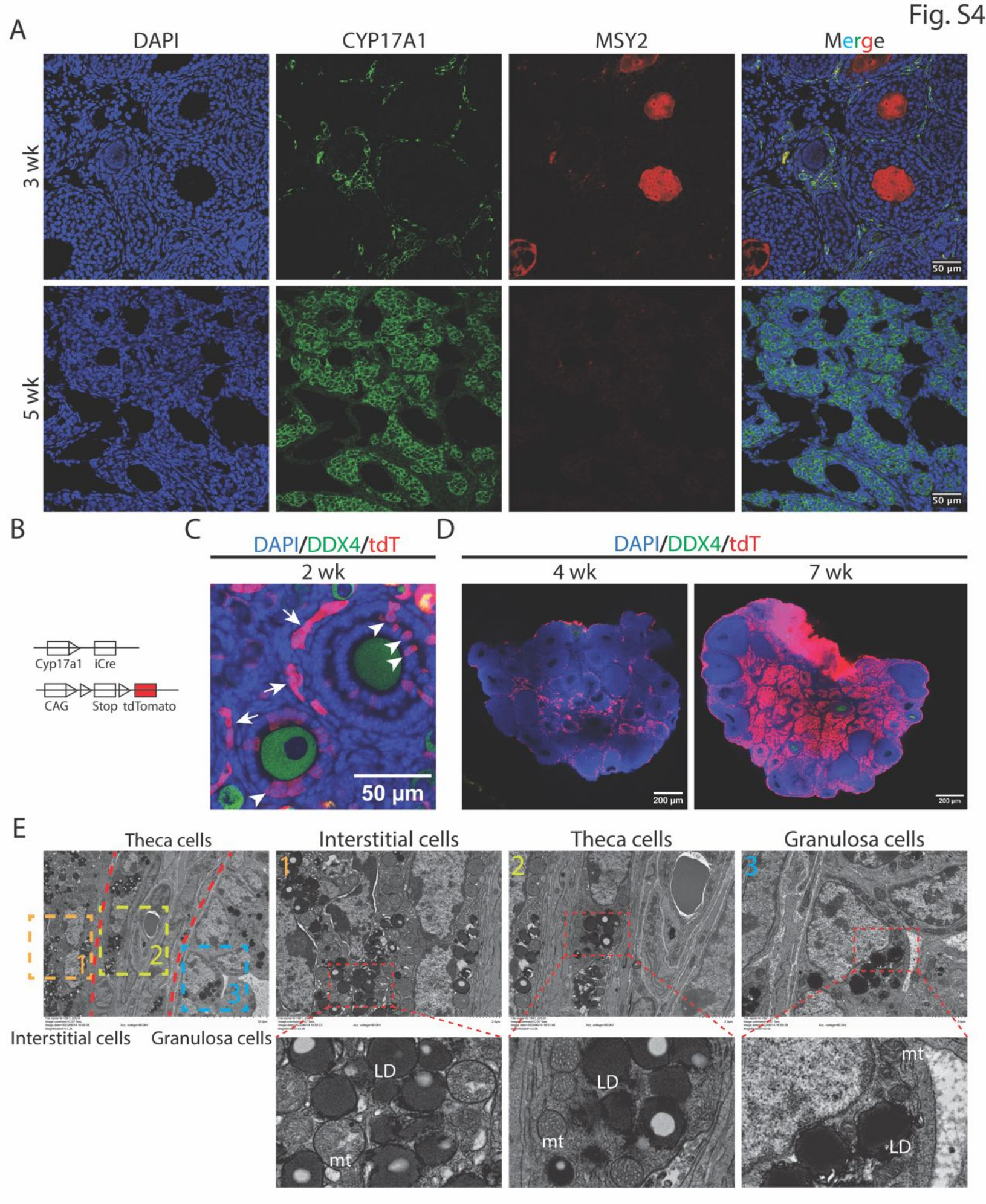
A
DAPI
CYP17A1
MSY2
Merge
3 wk
5 wk
50 µm
50 µm
B
Cyp17a1
iCre
CAG
Stop
tdTomato
C
DAPI/DDX4/tdT
2 wk
50 µm
D
DAPI/DDX4/tdT
4 wk
7 wk
200 µm
200 µm
E
Theca cells
Interstitial cells
Theca cells
Granulosa cells
1
2
3
Interstitial cells
Granulosa cells
LD
mt
LD
mt
mt
LD

Fig. S5

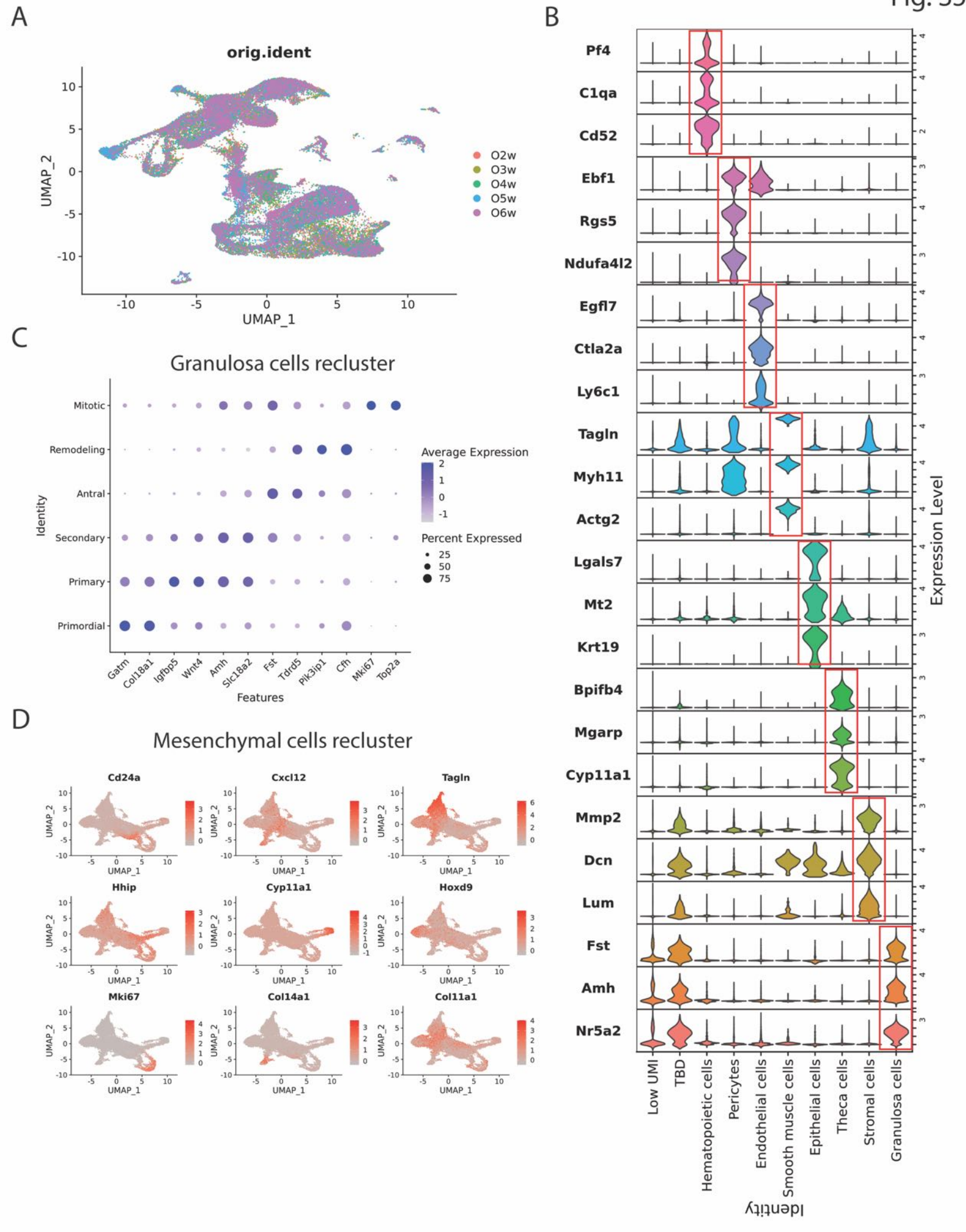
A
orig.ident
UMAP_2
UMAP_1
O2w
O3w
O4w
O5w
O6w
B
Pf4
C1qa
Cd52
Ebf1
Rgs5
Ndufa4l2
Egfl7
Ctla2a
Ly6c1
Tagln
Myh11
Actg2
Lgals7
Mt2
Krt19
Bpifb4
Mgarp
Cyp11a1
Mmp2
Dcn
Lum
Fst
Amh
Nr5a2
Expression Level
Low UMI
TBD
Hematopoietic cells
Pericytes
Endothelial cells
Smooth muscle cells
Epithelial cells
Theca cells
Stromal cells
Granulosa cells
Identity
C
Granulosa cells recluster
Mitotic
Remodeling
Antral
Secondary
Primary
Primordial
Identity
Average Expression
Percent Expressed
Gatm
Col18a1
Igfbp5
Wnt4
Amh
Slc18a2
Fst
Tdrd5
Pik3ip1
Cfh
Mki67
Top2a
Features
D
Mesenchymal cells recluster
Cd24a
Cxcl12
Tagln
Hhip
Cyp11a1
Hoxd9
Mki67
Col14a1
Col11a1
UMAP_1
UMAP_2

Fig. S6

A

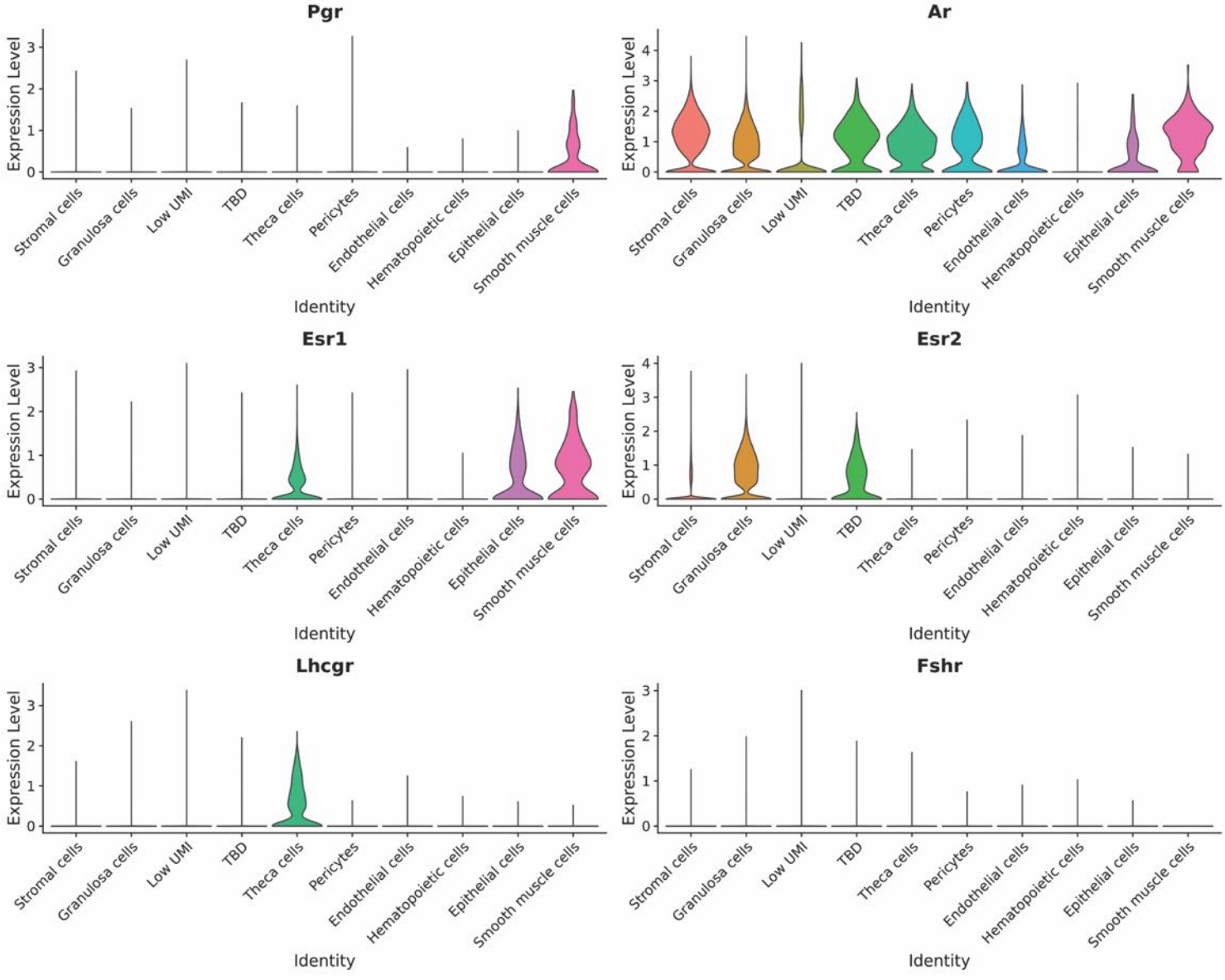
Pgr
Ar
Esr1
Esr2
Lhcgr
Fshr
Expression Level
Identity
Stromal cells
Granulosa cells
Low UMI
TBD
Theca cells
Pericytes
Endothelial cells
Hematopoietic cells
Epithelial cells
Smooth muscle cells

B

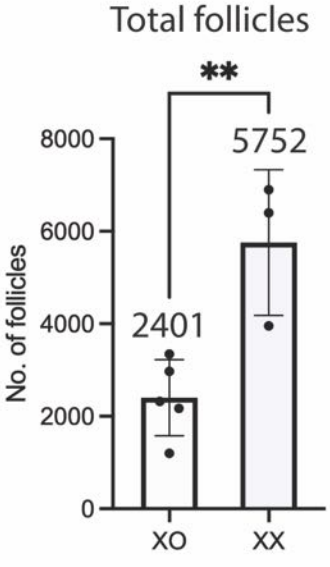
Total follicles
**
5752
2401
No. of follicles
8000
6000
4000
2000
0
XO
XX

C

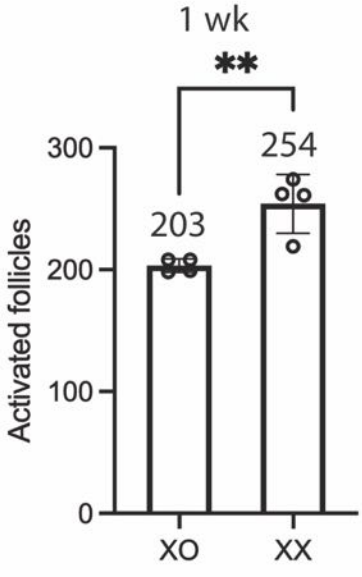
1 wk
**
254
203
Activated follicles
300
200
100
0
XO
XX

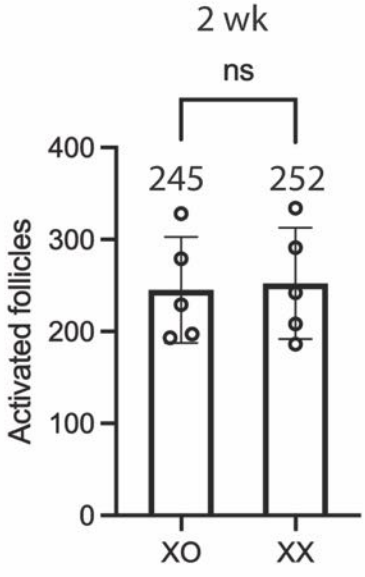
2 wk
ns
245
252
Activated follicles
400
300
200
100
0
XO
XX